EVIDENCE OF PRESSURE DEPENDENT PERMEABILITY IN LONG-TERM

SHALE GAS PRODUCTION AND PRESSURE TRANSIENT RESPONSES

A Thesis

by

FABIAN ELIAS VERA ROSALES

Submitted to the Office of Graduate Studies of
Texas A&M University
in partial fulfillment of the requirements for the degree of

MASTER OF SCIENCE

Approved by:

Chair of Committee,   Christine Ehlig-Economides
Committee Members,   Robert Wattenbarger
                       Maria Barrufet
Head of Department,   Dan Hill

December 2012

Major Subject: Petroleum Engineering

ABSTRACT

The current state of shale gas reservoir dynamics demands understanding long-term production, and existing models that address important parameters like fracture half-length, permeability, and stimulated shale volume assume constant permeability. Petroleum geologists suggest that observed steep declining rates may involve pressure-dependent permeability (PDP).

This study accounts for PDP in three potential shale media: the shale matrix, the existing natural fractures, and the created hydraulic fractures. Sensitivity studies comparing expected long-term rate and pressure production behavior with and without PDP show that these two are distinct when presented as a sequence of coupled build-up rate-normalized pressure (BU-RNP) and its logarithmic derivative, making PDP a recognizable trend.

Pressure and rate field data demonstrate evidence of PDP only in Horn River and Haynesville but not in Fayetteville shale. While the presence of PDP did not seem to impact the long term recovery forecast, it is possible to determine whether the observed behavior relates to change in hydraulic fracture conductivity or to change in fracture network permeability. As well, it provides insight on whether apparent fracture networks relate to an existing natural fracture network in the shale or to a fracture network induced during hydraulic fracturing.

DEDICATION

To the lord, our God.

To my current and future family, on earth and heaven.

To my city, Guayaquil, and my homeland, Ecuador

To my father and to my mother.

ACKNOWLEDGEMENTS

NOMENCLATURE

A	=	Area, acre
b	=	Fracture width, ft
c_f	=	Initial rock compressibility, 1/psi
c_g	=	Initial gas compressibility, 1/psi
c_t	=	Initial total compressibility, 1/psi
c_w	=	Initial water compressibility, 1/psi
C_{fD}	=	Dimensionless hydraulic fracture conductivity
h	=	Formation thickness, ft
k	=	Formation permeability, md
$k_f w$	=	Fracture conductivity, md-ft
L_w	=	Horizontal well length, ft
$m(p)$	=	Real gas pseudopressure, psi$_2$/cp
n_F	=	Number of hydraulic fractures
p_i	=	Initial pressure at formation depth, psi
p_{wD}	=	Dimensionless bottomhole flowing pressure
p_{wf}	=	Bottomhole flowing pressure, psi
Q	=	Cumulative production, scf
q	=	Gas production rate, Mscf/d
rw	=	wellbore radius
s_g	=	Gas saturation, fraction
T	=	Time, hr
T	=	Formation temperature, °F

tDxF	=	Dimensionless time respect to fracture half-length
t_e	=	Material balance time, hr
$t_{e,\ elf}$	=	End of linear flow material balance time, hr
t_{elf}	=	End of linear flow actual time, hr
V	=	Volume, ft^3
V_p	=	Pore Volume, ft^3
x_F	=	Hydraulic fracture half-length, ft
x_s	=	Hydraulic fractures spacing, ft
z_w	=	Vertical distance to lower boundary, ft

Greek Variables

ϕ	=	Porosity, fraction
μ	=	Gas viscosity, cp
∂_p	=	Derivate with respect to pressure
∇	=	Diffusivity
α	=	Exponential decay factor

Subscripts

D	=	Dimensionless
e	=	Material balance time
elf	=	End of linear flow
i	=	Initial
p	=	Constant pressure
R	=	Constant rate

TABLE OF CONTENTS

LIST OF FIGURES

LIST OF TABLES

CHAPTER I

INTRODUCTION

Shale gas reservoir systems and their characterization have been shaping industry trends on petroleum engineering and current works are trying to understand how these systems behave during production life. The big challenge of shale reservoirs systems is they do keep a dynamic behavior and their modeling becomes complex through their long-term production performance.

1.1 Problem Descriptions

Engineering professionals have reported that most of slip decay in production in some shale reservoirs is because of a phenomenon called pressure dependent permeability. The big discrepancy is in which part of the shale reservoir system, the matrix, the existing natural fractures of the hydraulic fractures, the phenomenon takes place in.

A possible modeling solution is a dynamic characterization of the hydraulic fractures and its finite conductivity that may experience decay because of overpressure stress regimes affecting the reservoir. The role of hydraulic fractures to transmit the fluid from a tight rock is elemental for an economic production in these shale systems.

Another possible answer is the variable value of natural fracture permeability from the shale system. As the matrix shows extreme low values, is the network of existing fractures that provide most of the feed for production and suffer most of the PDP through the production life.

The solution of this complex scenario is whether we can report absolute evidence of pressure dependent permeability in shale gas reservoir performance. Either by analyzing flow regimes showing unit slope, linear or bilinear in pressure transient analysis or production analysis, unique characterization solution becomes challenging when only one or likely two of those flow regimes are present in the performance of such hydraulic fractured wells.

To solve such engineering doubts, confident and proven dynamic methods are used to diminish the uncertainty of characterizing flow regimes. Furthermore, complete understanding of such flow regimes is required for an unbiased diagnosis.

1.2 Objectives

The first objective of this work is to investigate the influence of pressure dependent permeability in the stimulated reservoir volume characterization and its effect in the estimated ultimate recovery when constant parametric models are contrasted with variable models.

The second objective is to show the causes of PDP and how to recognize them for a better surveillance of long-term reservoir performance.

1.3 Methodology

This investigation specifies its scope on homogeneous and dual porosity models for multi-traverse fractures shale gas wells with constant and variable permeability parameters. Early time flow regime analysis is presented in both pressure and production transient analysis by first showing sensitivity analysis with common shale gas properties

and later applied on actual reservoir performance, including shale formations from Fayeteville, Haynesville and Horn River.

In the end, conclusions are presented either capturing or not the pressure dependent permeability in the dynamic behavior of hydraulic fractured shale gas wells in each analyzed formation.

1.4 Organization of this Thesis

Chapter I: Introduction – it describes the current problem to be solved and the objective of study, giving insights of the objectives, methodologies and key features of the thesis.

Chapter II: Literature analysis – providing with analysis of current and previous engineering works on the field. Most of investigation on pressure dependent permeability has been focused on sandstone and matrix only, some of them in hydraulic fractures and their aperture and effective length. The model available in the selected commercial software is also reviewed and the phenomenon of pressure dependent permeability is discussed.

Chapter III: Sensitivity studies on Pressure-Dependent-Permeability – these chapters focus on the phenomenon using production data analysis and pressure transient analysis to investigate its behavior in shale reservoirs Expected flow regimes explanation and Pressure dependent permeability is discussed.

Chapter IV: Field studies on Pressure-Dependent-Permeability – these chapters focus on the Fayetteville, Haynesville and Horn River shales by addressing important parameters using homogeneous and pressure dependent models. Expected flow regimes

are explained and model matches are suggested. The Pressure dependent permeability is discussed.

Chapter V: Conclusions and recommendations: the purpose of this chapter is to compile the ideas developed in this thesis by contrasting similarities and discussing the most likely origins of pressure-dependent-permeability. Observations and recommendations towards improved reservoir characterization are introduced.

CHAPTER II

LITERATURE REVIEW

The objective of this chapter is to provide background on studies and analytical flow models that can be employed to identify evidence of pressure-dependent-permeability (PDP) in pressure and production transient data. In the following sections, matrix, hydraulic fracture and natural fracture PDP will be addressed. A final section explains techniques that have been used to detect the presence of PDP in transient data.

2.1 Matrix-PDP

Varoigs and Rhoades (1973) simulated buildup behavior for conventional gas sandstone reservoirs to investigate PDP behavior. Their model indicated that conventional Horner analysis would indicate a flow capacity (kh) value 10% lower than true initial values and apparent skin values not caused by physical damage but only by permeability reduction around the wellbore. Figure 2.1 shows two simulated buildup cases at different drawdown times where damage is present, one with skin factor of 1 and other of -3 at and its results indicates skin factors because of permeability reduction alone are not strictly additive. Such mechanical obstruction generates an additional decrease in permeability at early time that decreases at later times. They also showed that effects of stimulation seem to override stress-sensitivity effects. In both cases, (kh) determination will be nearly correct at early time and decrease with time.
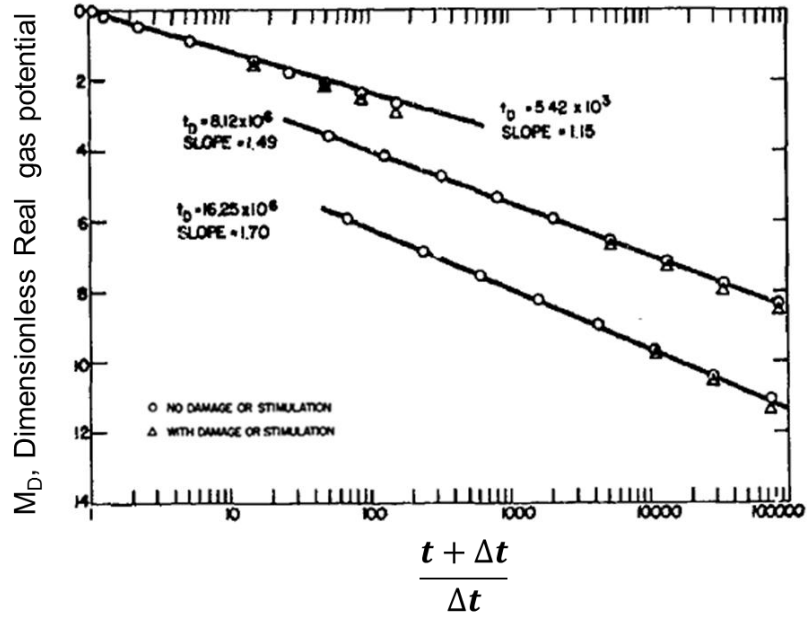
Figure 2.1: Horner plots at different drawdown times.

Later, Samaniego et al. (1977) investigated PDP using Eq. 1 to describe flow in the reservoir where diffusivity is pressure-dependent.

$$\nabla^2 m(p) = \frac{\phi(p)\mu(p)c_t(p)}{k(p)} \frac{\partial m(p)}{\partial t} \dots\dots\dots\dots\dots\dots\dots\dots\dots\dots\dots\dots\dots\dots\dots(1)$$

where

$$m(p) = \int_{P_m}^{p} \frac{k(p)\rho(p)}{[1-\phi(p)]\mu(p)} \partial p \dots\dots\dots\dots\dots\dots\dots\dots\dots\dots\dots\dots\dots(2)$$

They also determined that for buildup dimensionless solutions, constant property and pressure-dependent equations were the same for practical purposes, making appear that principle of superposition was valid also for pressure-dependent flow. The kh estimation was close to kh at average pressure rather than initial pressure when buildup solutions were analyzed in terms of pressure than pseudopressure with an error of 7%.

6

Evers and Soeiinah (1977) used the model by Varoigs and Rhoades (1973) to investigate the effect on transient test analysis and long term performance of permeability changes due to stress variation over the producing life of a reservoir. They determined that stress-sensitive behavior during transient testing can be confused with or masked by the presence of turbulence and viscosity changes and buildup tests during the first few years of production definitively confirm its presence or absence. Walsh (1981) confirmed by numerical and field experiments that the effect on flow rate of independent changes in pore and confining pressure can be summed as in Figure 2.2.
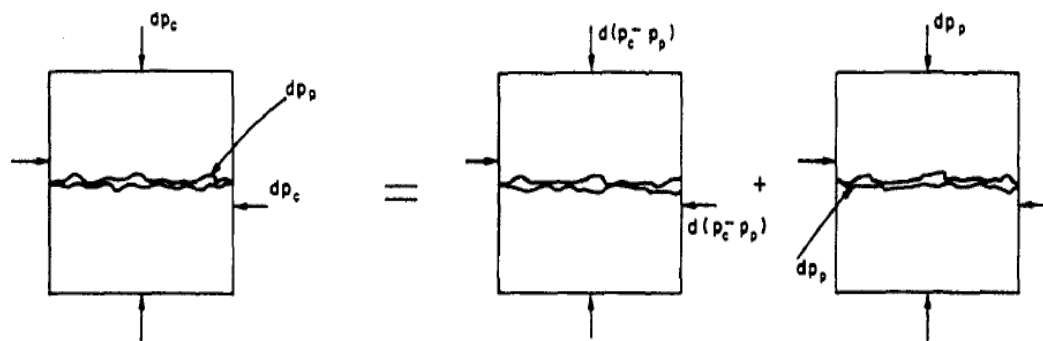
Figure 2.2: Effective external stress acting on a reservoir.

Later, numerical studies by Kikani and Pedrosa (1991) gave solutions into pressure transient behavior by defining a permeability modulus shown on Eq. 3 that accounts for changes in the pressure and captures the exponential decay behavior that has been recorded on several core experiments.

$$k(p) = e^{-\alpha(P_i - P)} \dots\dots\dots\dots\dots\dots\dots\dots\dots\dots\dots\dots\dots\dots\dots\dots\dots\dots(3)$$

Studies by Franquet and Rodriguez (2004; 2004) developed tight gas solutions that indicated that under PDP conditions calculations for original gas in place (OGIP) were under-estimated, and the productivity index at the end of the transient period is reduced.

2.2 Hydraulic Fracture-PDP

It is very well known and understood that weak proppant materials can be crushed under increasing stress as the pore pressure declines (Economides et al. 2002).To avoid loss of hydraulic fracture conductivity over time, they explain the importance of considering strength in proppant selection whenever the fracture is expected to undergo increasing effective stress overthe life of the well. Figure 2.3 shows data measured by Miller, Conway and Salter (2010) quantifying propped fracture conductivity as a function of stress for three types of proppant.
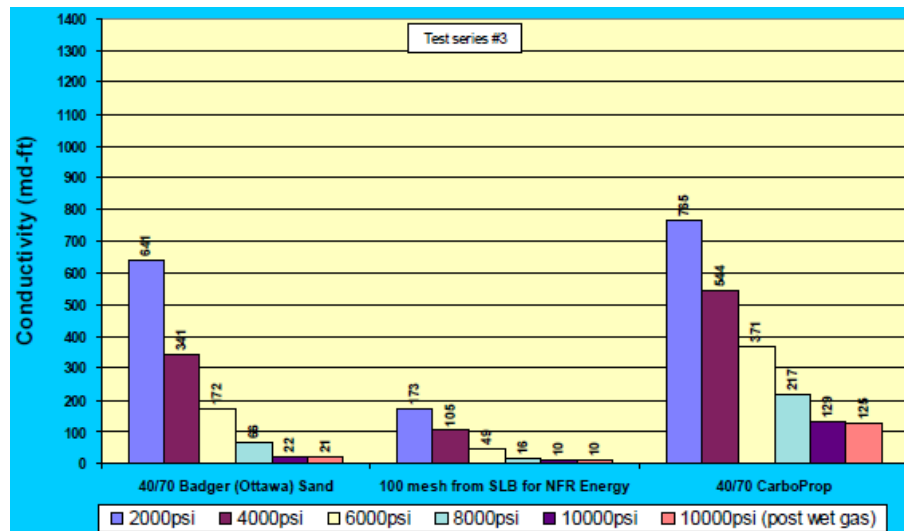
Figure 2.3: Propped fracture conductivity as a function of stress

Similarly, Abass et al. 2007 indicated that waterfracs using low proppant concentration are used in shale wells because fines generated from proppant crushed under stress may reduce the conductivity of the hydraulic fractures.

Laboratory studies by Weaver, Richman and Luo (2010) show that geochemical proppant degradation is not trivial but occurs as a function of closure stress on the proppant and the temperature to which the proppant is exposed. The degree to which subsequent remineralization in the proppant pack leads directly to the loss of hydraulic fracture permeability depends on the composition of both the proppant material and the formation material. Under some conditions this may account for as much as 90% of observed productivity loss, as seen in Figure 2.4.
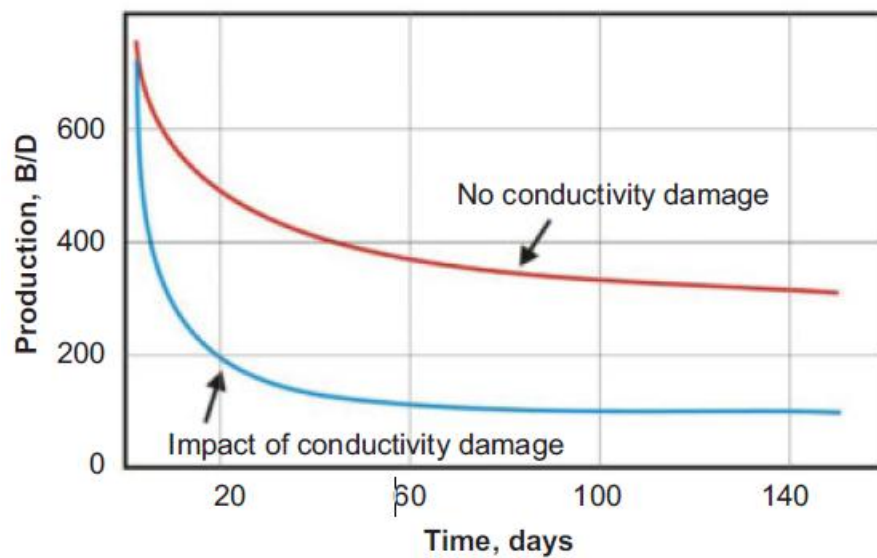
Figure 2.4: Effect of conductivity on long-term production

2.3 Natural Fracture-PDP

Ostensen (1986) discussed a pressure-dependent-permeability (PDP) phenomenon by experimental core analysis and numerical modeling, in which initial steady-state deliverability was reduced as much as 30% as the average reservoir pressure dropped, and the steady-state productivity was controlled by the average of the stress-dependent permeability over the pseudo-pressure drawdown. Figure 2.5 is a graph of the relative gas production rate given by the ratio of the simulated gas rate to the initial rate versus the intercept stress shows that the effect was increased at greater depth in response to increasing vertical stress. Intercept stress Figure 3 axes means the physical property of the rock that depends on the smoothness of the crack faces where smoother faces leads to lower intercept stress, which causes larger stress sensitivity.
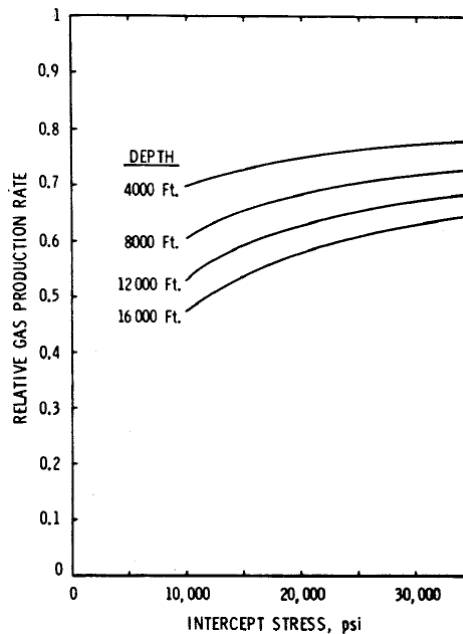
Figure 2.5: Reduction of initial gas production rate because of PDP presence

Gale et al. (2007) reported the presence of natural fractures in shale formations, specifically in the Barnet Shale. Their study indicated that natural and regionally developed, opening-mode fractures may be reopened during hydraulic fracture treatments, providing a larger rock volume in contact with the wellbore as shown in Figure 2.6. Although most natural fractures observed in the Barnett formation samples are sealed, cements in the fractures that are not generally template onto grains in the wall rock may allow the fractures to act as planes of weakness that can reactivate.
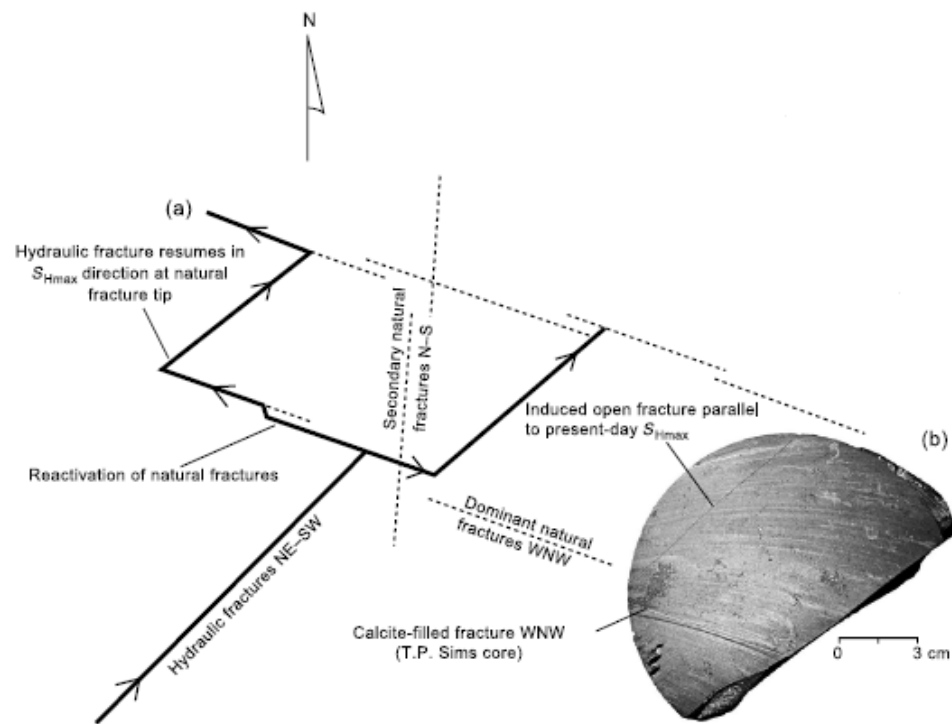
Figure 2.6: Importance of natural fracture system for optimal stimulation

In fractured reservoirs, there are pre-existing fractures and faults at variable orientations. Zoback et al. (2012) states that slow slip on pre-existing fractures is likely to be a fundamental component of hydraulic stimulation and may induce slip on mis-oriented faults only as rapidly as pore pressure propagates along it. As time goes on and injection pressure spreads out along fractures the slip velocity may increase as well as the amount of displacement, in turn affecting the stress of the reservoir. In-situ stress has to be a factor to measure because its variation leads to different interactions on permeability changes making the fractures to dilate during injection and close during drawdown, especially in tight, overpressured reservoirs (Lorenz 1999).

To account for stress sensitivities, Tao et al (2009) developed a fully coupled poroelastic displacement discontinuity model showing that permeability of a natural fracture system can be sensitive to stress changes during production. In an isotropic stress condition, fracture deformation is dominated by compression and the shear deformation and dilation can be neglected. In this case, the fracture permeability will be reduced according to the cubic law of production shown on Eq. 4.

$$k_f = \frac{n_f w_f^2}{12}$$ ……………………………………………………………………………(4)

where n_f is the fracture frequency defined as fractures per unit length. This study showed that natural fracture permeability decline with production is evident in buildup tests as Figure 2.7 illustrates.
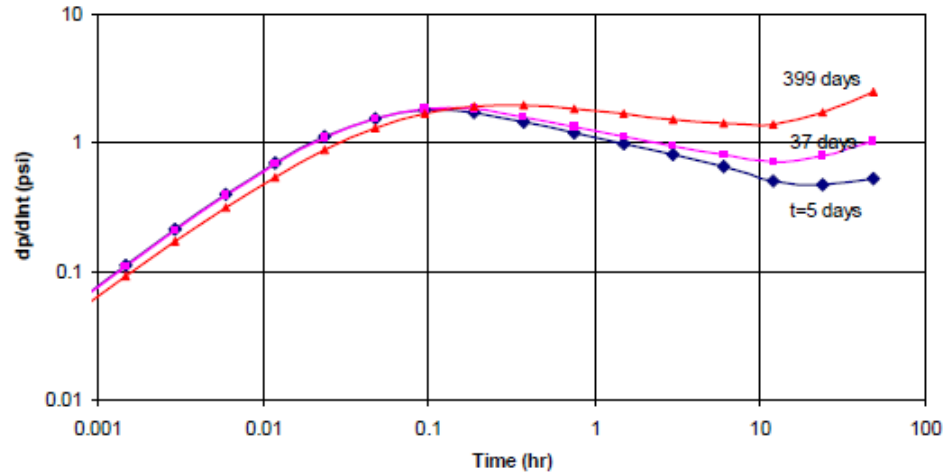
Figure 2.7: Log-log plot showing decrease of the natural fracture permeability

Tao et al. (2009) further indicates that when anisotropic stress conditions are present, shear fracture deformation is approximately linear before yielding, and shear stiffness is abruptly reduced to zero after yielding. There are some reservoirs that are already at the critical stress conditions and the fractures are already yielded, indicating very week fractures for which a disturbance of shear stress can result in large shear deformation that induces normal deformation by dilation. This scenario may enhance the fracture conductivity and make the permeability of the natural fracture to increase as shown in Figure 2.8. If stress contrast between the maximum and minimum principal stress is not high enough to make the fractures yielding, then production will reduce the overall fracture permeability.
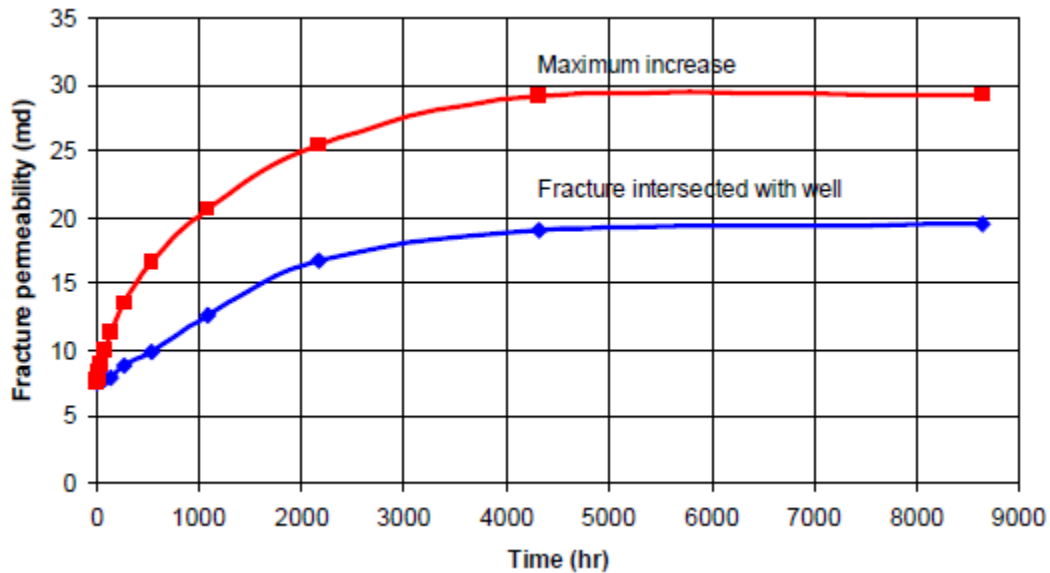
Figure 2.8: Increment of fracture permeability from initial conditions.

This physical behavior was reported by Warpinski (1991) on two scenarios where the natural fractures are normal to the maximum stress or are subparallel to the maximum stress. The resultant permeability is given as a function of the net stress on the natural fractures and for hydraulic fracturing purposes, increased permeability occurs when the net stress decreases, hence increasing the leakoff coefficient.

2.4 Detecting the Presence of PDP in Transient Pressure and Production Data

Application of pressure transient data is fairly known to detect reservoir changes, especially in offshore reservoirs. Petro et al. (1997) used successive pressure buildups to identify, characterize and quantify the loss of formation flow capacity in turbidite sands of the Gulf of Mexico. In such work, reservoir compaction leaded to fines generation which resulted in near wellbore damage and well deliverabilities were reduced up to

70%. Later, Guenther et al (2005) used successive buildups to quantify the reduction in flow capacity of a gas condensate field in a 1.8 year period. Recently, Pan et al. (2011) used successive buildups acquired through the production time of the well to show evidence of subsidence in a medium oil brazilian offshore reservoir. To date no evidence in literature suggests application of the successive buildup analysis technique in shale reservoirs.

The use of material balance time (t_e) and pressure normalized rate (PNR) defined as instantaneous productivity index allows the long-term production data to be seen as a single virtual rate decline at constant pressure Palacio and Blasingame (1993). In this study, rate normalized pressure (RNP), which is defined as reciprocal of the instantaneous productivity index, will be used to analyzes long-term production data as a virtual pressure drawdown at constant rate when graphed versus the material balance time. Note that the constant rate condition is more favorable for flow regime investigation because it shows characteristic slopes when viewed as the derivative of the pressure change with respect to the natural log of time. Therefore, RNP and RNP derivative (RNP') will be used to investigate the flow regimes. Eq. 5 and Eq. 6 show the definitions for RNP and RNP' when pseudopressure function, m(p), is used.

$$RNP = \frac{m(p_i) - m(p_{wf})}{q}$$ ....(5)

$$RNP' = \frac{dRNP}{dlnt_e} = \frac{d[m(p_i) - m(p_{wf})]/q}{dlnt_e}$$ ....(6)

The single porosity model represents flow behaviors of MTFHW producing from homogeneous or single porosity reservoir without any opened, reopened, or natural fractures. Song and Ehlig-Economides (2011) presented a sequence of flow regimes for

15

the MTFHW production on log-log rate normalized pressure (RNP) and its derivative (RNP') versus material balance time (t_e). Five flow regimes are shown in Figure 2.9 including pseudolinear flow (PL) normal to hydraulic fractures, pseudo pseudosteady state flow (PPSS) indicating interference boundary between two fractures, compound linear flow with production from beyond fracture tips, pseudoradial flow, and drainage boundary behavior induced by the well spacing. They also show the field examples from Fayetteville, Haynesville, and New Albany shale with the Haynesville shale example show only PPSS and the New Albany shale example show only PL while the Fayetteville shale example shows both PL and PPSS flow regimes.
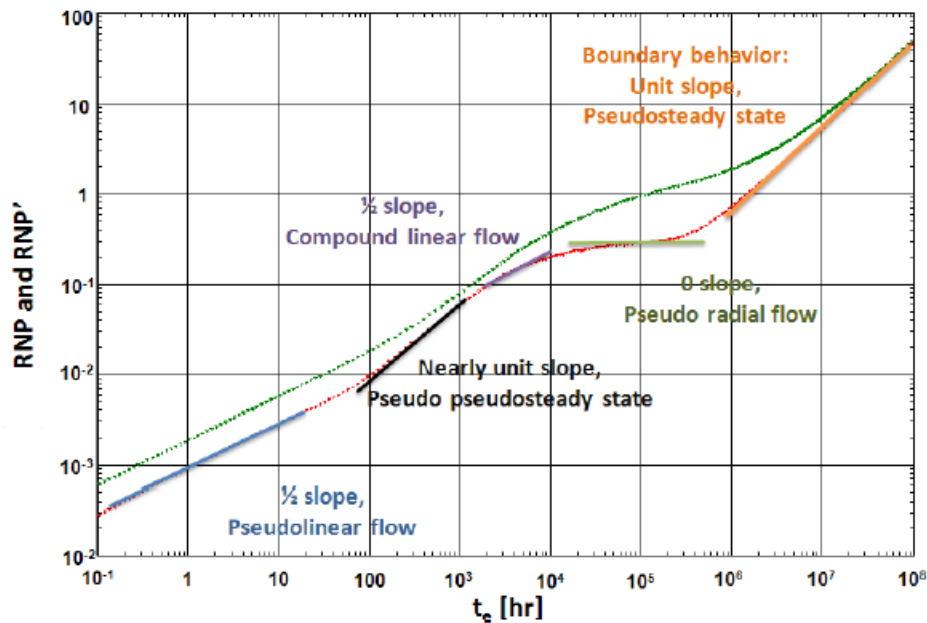
Figure 2.9: Sequence of flow regimes in a rate-normalized pressure log-log plot.

16

This study provided an equation to calculate the parameters when PL regime is observed. Eq. 7 and Eq. 8 can be used for gas when pseudopressure function, m(p), is used.

$$RNP = \frac{40.93T}{n_F h x_F \sqrt{k} \sqrt{(\phi \mu c_t)_i}} \sqrt{t} \dots\dots\dots\dots\dots\dots\dots\dots\dots\dots\dots\dots\dots\dots\dots\dots\dots\dots\dots\dots\dots\dots (7)$$

$$RNP' = \frac{1}{2} \left[\frac{40.93T}{n_F h x_F \sqrt{k} \sqrt{(\phi \mu c_t)_i}} \sqrt{t} \right] \dots\dots\dots\dots\dots\dots\dots\dots\dots\dots\dots\dots\dots\dots\dots\dots\dots (8)$$

Eq. 7 and 8 also indicate that MTFHW will exhibit a 1/2 slope straight line for both RNP and RNP' on log-log plots versus material balance time during the formation pseudolinear flow regime. Also, it emphasizes that the RNP and RNP' will be separated by a factor of two (2) when fracture skin is negligible.

A coupled BU-RNP introduced by Ehlig-Economides et al. (2009) will allow for a chronological sequence of flow regimes and changing reservoir conditions during its performance. This is achieved by multiplying the RNP and RNP' response by the flow rate just before the selected buildup. In consequence, the long response from the production analysis is bonded with the early time response of the buildup and connecting the flow regimes of the reservoir for their respective quantification. This unified approach allows continuous monitoring of production and pressure from individual wells and as it relies on drawdown trends, it is more amenable to automated model selection and it will be used to identify, characterize and quantify the dynamics of shale reservoirs in this study.

2.5 Objectives

This work focuses on identifying whether the presence of pressure dependent permeability is evident in shale reservoirs, characterizing the pressure and production transient response, and quantifying the permeability or conductivity variation in the shale formation and its impact on reservoir performance.

2.6 Methodology

Fracture conductivity loss or effective permeability change is evident only after sufficient pressure change has occurred to cause a detectable change. In the immediate vicinity of the well high pressure gradients in tight formations may induce fracture conductivity and/or permeability variations in long term production transient behavior that might be detectable in PNR or RNP data presentations. Hence, this work will include sensitivity analysis using available models to evaluate what might be seen in transient production data.

In addition, this study will use the strategy of analyzing sequential rate-normalized buildup transients as indicated by Pan et al. (2011). Sequential rate-normalized buildup analysis has not been reported to calculate dynamics on the stimulated reservoir volume (SRV). Analysis of synthetic data will demonstrate the approach that will then be illustrated using field data.

2.7 Organization of this Thesis

Six chapters are planned for this thesis. The details of each chapter are as follows:

Chapter I: Introduction - this chapter will give information about problem description, general idea to the problem, objectives, methodology, and organization of the thesis.

Chapter II: Literature survey - this chapter will provide a brief review of the pressure dependent permeability and its effect on the matrix, hydraulic fractures and natural fracture network. Description of current and novel methodology to acquire, analyze and characterize this phenomena and its influence on the well fracture performance on homogeneous reservoirs

Chapter III: Sensitivity Studies on Pressure-Dependent-Permeability – this chapter will use existing models to show that evidence of PDP can be detected in transient pressure data in the form of successive pressure buildups and in production data as distinctive trends in the RNP derivative.

Chapter IV: Field Studies on Pressure-Dependent-Permeability – this chapter will show presence or absence of PDP in Fayetteville, Haynesville and Horn River shales. Observed flow regimes are explained, model matches with data are shown, and PDP is discussed.

Chapter V: Conclusions and recommendations - this chapter will conclude all the findings and ideas developed throughout the thesis. Observation and recommendation of how this work can improved future reservoir characterization efforts is included.

CHAPTER III

SENSITIVITY STUDIES ON PRESSURE-DEPENDENT-PERMEABILITY

Chapter II provided a literature review on PDP in shale reservoirs. This chapter illustrates how this phenomenon manifests in pressure transient analysis (PTA) and production data analysis (PDA). Sensitivity studies using exponential decline also demonstrate similarities and key differences when fracture permeability, matrix permeability are under the influence of PDP in long term production and early transient time.

This chapter also shows how PDP impacts future production and implications on 30 diagnoses.

The sensitivity analyses in this study are based on a multistage transverse hydraulic fractured well (MTHFW) 4000 feet in length with 41 fractures spaced 100 ft apart. Matrix permeability, hydraulic fracture conductivity, and natural fracture network permeability sensitivities illustrate are investigated in the following sections. Table 3.1 shows essential input values for flowing gas sensitivity analyses considering exponential decay function in permeability.

It is necessary to highlight that only permeability from matrix and hydraulic fractures are object of this study. Sensitivities about viscosity or porosity dependent on permeability are not part of this discussion.

Table 3.1: Well parameters of synthetic model

Well Parameters		
L_w	4000	ft
h	300	ft
z_w	150	ft
n_f	41	
p_i	5000	psia
x_f	300	ft
k	100	nd
ϕ	0.1	
μ	0.0027	cp
Area	101.01	acre
V_p	$3.3 \bullet 10^8$	ft^3

3.1 Long Term Production Sensitivity Analysis

The rate-normalized pressure (RNP) derivative described in Chapter II is used to visualize the flow regime behavior for different parameter value combinations in the long term production analysis. Infinite and Finite conductivity will consider different analysis in this section for both matrix PDP (M-PDP) and hydraulic facture PDP (HF-PDP).

3.1.1 Matrix-PDP Cases

Chapter II describes exponential permeability decline as one way to model matrix PDP (M-PDP). Only changes in the effective permeability using exponential values are considered in the following pages. Interestingly, flow regimes will show similar behaviors as those with constant permeability values but as exponent values changes, early appearance of unit slope will manifest as higher values enters the sensitivity.

3.1.1.1 M-PDP Finite Conductive Fracture Case

Figure 3.1 shows the impact of the exponent in the PDP model for finite conductivity hydraulic fractures with dimensionless conductivity 10.

Increasing decline exponent corresponds to greater permeability decrease, and increasingly higher derivative level. For the same initial permeability, the spread between the derivative curves increases over time. The transition from bilinear flow seen as ¼ slope to linear flow seen as ½ slope occurs earlier for greater permeability decline exponent because over time the fracture dimensionless conductivity increases as the matrix permeability decreases. The transition to pseudosteady-state behavior with unit slope occurs later for increasing permeability decline exponent, but ultimately all curves merge together on the same unit slope trend because this trend is directly dependent on the volume drained by the well. As an aid, lines with characteristic flow regime slopes are included on the graph.
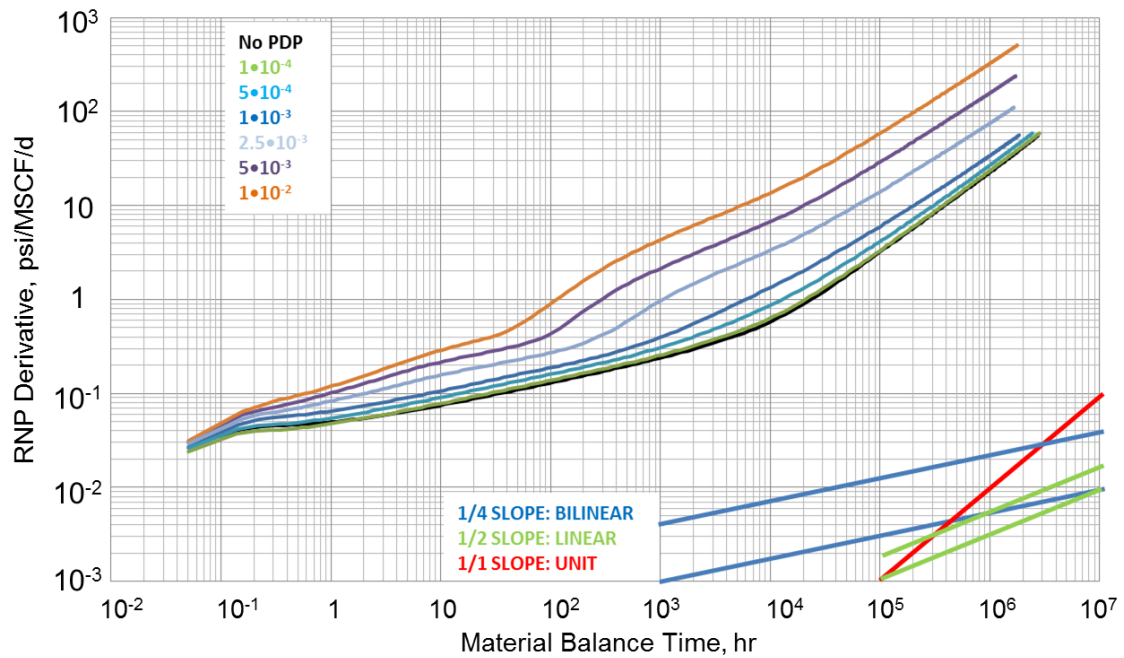
Figure 3.1: Increasing M-PDP and finite conductivity (C_{fD}=10) sensitivity

Figure 3.2 shows sensitivity to flowing pressures starting at initial pressure of 5000 psia and flowing from pressure differences of 1500 to 4500 psia for the same exponentially declining permeability with exponent value of $1 \cdot 10^{-3}$. Under PDP, lower flowing pressure reflects higher pressure drop from the formation pressure near the well and, therefore, lowers it permeability. This picture illustrates that the more the difference from initial pressure, the higher the level of the derivative when it is compared with the initial case of no PDP in the sensitivity. As before, all derivative curves tend to merge in late time to the same unit slope trend.
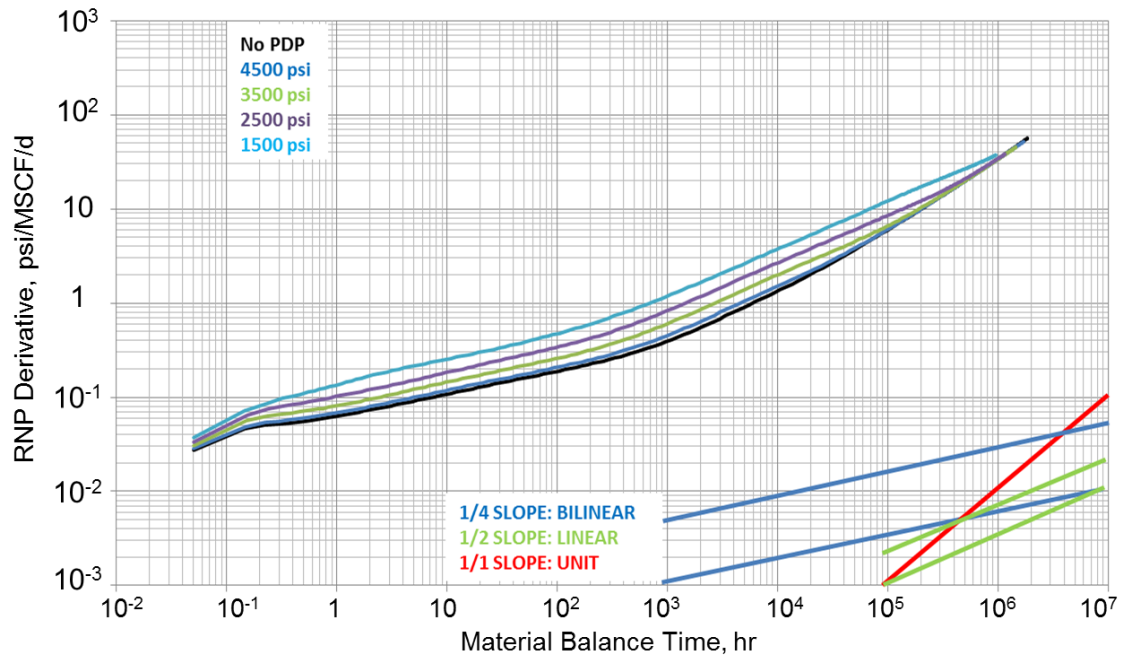
Figure 3.2: M-PDP finite conductive pressure difference sensitivity

These previous illustrations also show impact on well productivity index, which is the reciprocal of the RNP. Productivity index decreases until it reaches a final constant value at the start of pseudosteady state. Therefore, the greater the RNP value at the start of pseudosteady-state flow, the lower is the well productivity. Since well productivity is directly proportional to permeability, as the permeability declines, so will the well productivity index. Figure 3.3 illustrates this behavior translated on cumulative production over 30 years.
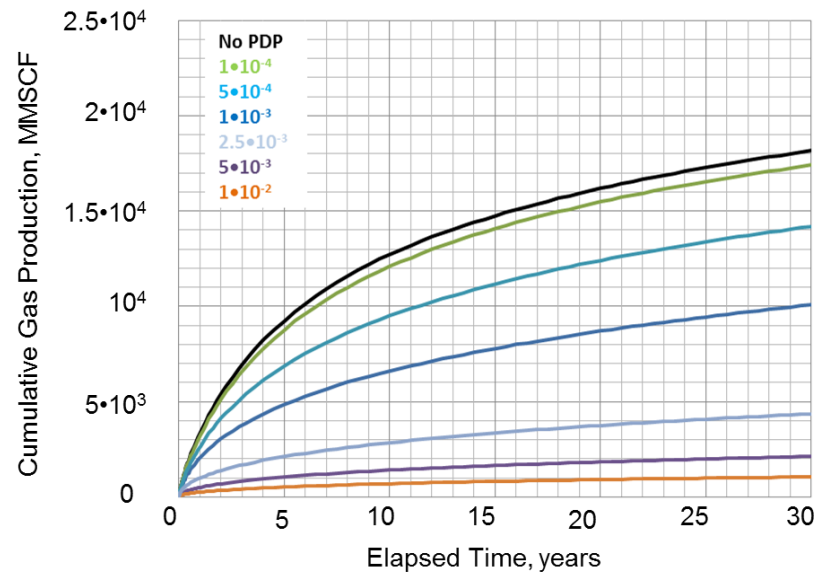
Figure 3.3: 30 year M-PDP finite conductivity production forecast

3.1.1.2 M-PDP Infinite Conductive Fracture Case

Figure 3.4 shows the same sensitivity as in Figure 3.1 but for hydraulic fracture dimensionless conductivity of 100.
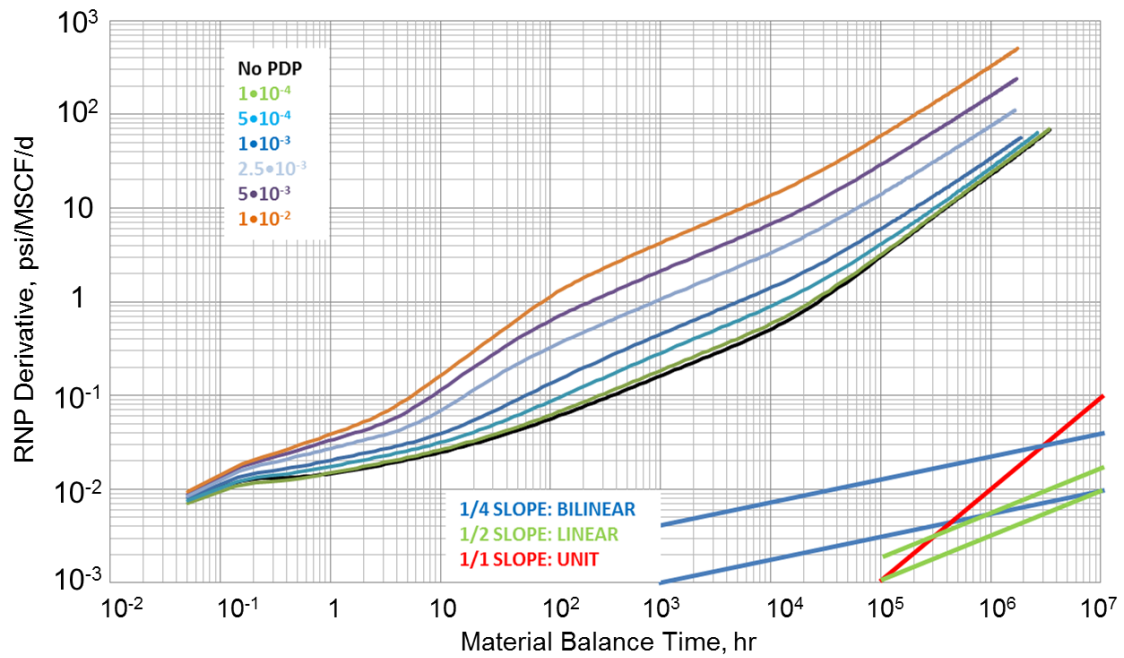
Figure 3.4: Increasing M-PDP and infinite conductivity (C_{fD}=100) sensitivity

The more the exponent decay factor increases in this case, the earlier the transition from bilinear to linear slope appears on the log-log plot. Figure 3.5 shows same sensitivity to flowing pressure as Figure 3.2. The transition between bilinear and linear flows remains the same but takes the linear flow longer to achieve unit slope as the derivative levels up with the difference of flowing pressure.
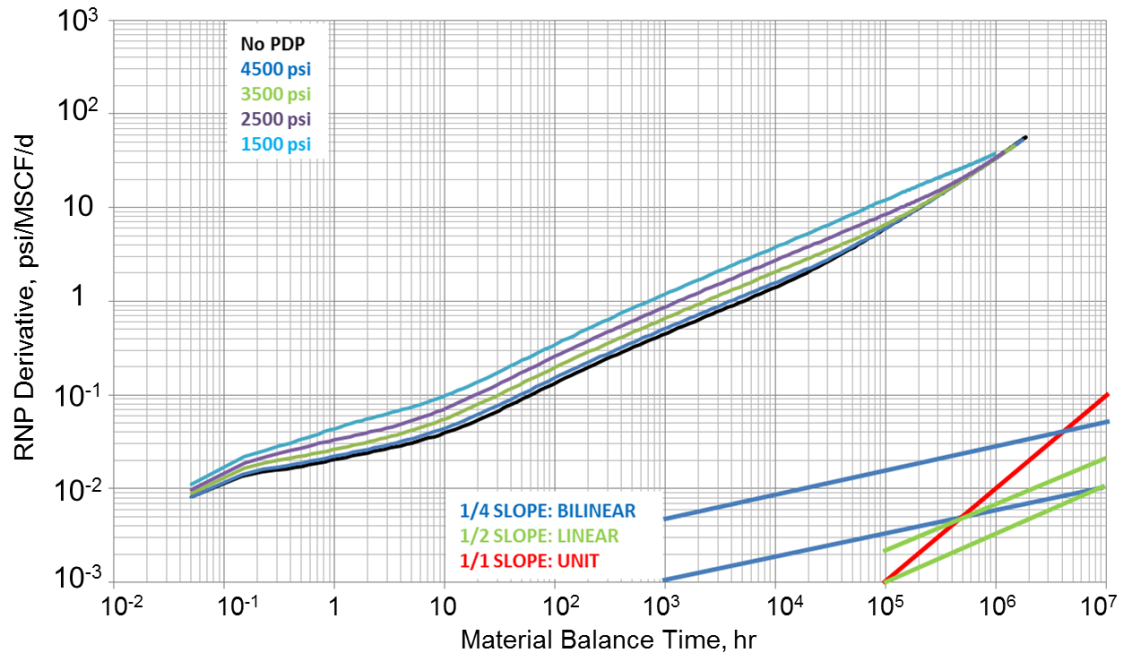
Figure 3.5: M-PDP infinite conductivity pressure difference sensitivity

Even more interesting is Figure 3.6 where production forecast includes these factors. Two scenarios show how the cumulative production displays different trends at 30 year forecast where the more the decrease, the lower the cumulative of production, in particular when higher exponents influences the decay in permeability. Curiously, the difference between each scenario is evenly away from each other but similar when the factors are as high as greater than $5 \cdot 10^{-3}$.
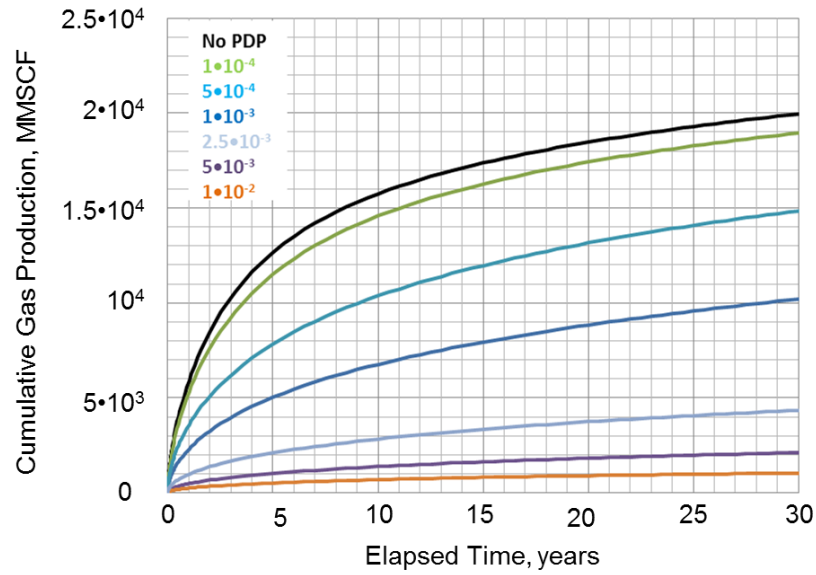
Figure 3.6: 30 year M-PDP finite conductivity production forecast

3.1.2 Hydraulic Fracture-PDP Sensitivity Cases

In this part of Chapter III, sensitivity studies considering hydraulic fracture-PDP (HF-PDP) with infinite conductive fractures and finite conductive fractures will reveal different behavior from those showed on previous figures considering M-PDP. Interesting to analyze is the reduction on production, made by HF-PDP, over time are comparable with the same reductions experienced on M-PDP but different flow behavior on log-log plots visualized with RNP.

3.1.2.1 HF-PDP with Infinite Conductive Fractures

In this section fracture conductivity is analyzed using the same parameters on table 3.1. Because the well is produced at constant pressure, the main effect is immediate conductivity lowering in the fractures to correspond to the permeability for the flowing pressure. However, the pressure gradient in each fracture is exaggerated by the permeability loss, making the apparent fracture conductivity even lower. Interestingly in

28

Figure 3.7, at higher exponent factor above $5 \cdot 10^{-3}$ a valley manifests in the RNP derivative with a similar shape of a pseudo steady dual porosity which may represent the presence of an outside reservoir dominating the flow from the shale at longer times.

Figure 3.7: Increasing HF-PDP and infinite conductivity (C_{fD}=100) sensitivity

As the same case with matrix sensitivity, hydraulic fracture permeability also experiences a rise in its pressure derivative depending on the magnitude of drop between the initial and flowing pressures represented in Figure 3.8. As before, the more the difference from initial pressure, the higher the level of the derivative when it is compared with the base case of constant permeability. This graphic in particular shows

all flow regimes begin with a bilinear flow which converges towards unit, the higher the drop in flowing pressure, the later its unit slope manifests and also shows that at very small conductivities, the linear flow represent with a ½ slope can be skipped from the derivative.
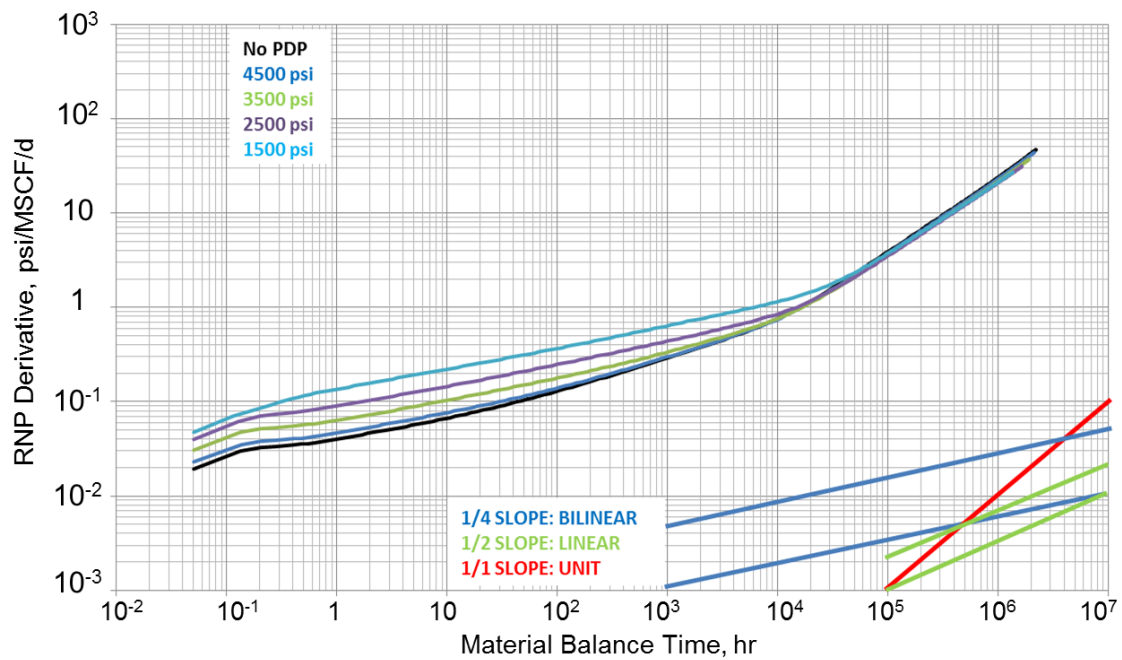
Figure 3.8: HF-PDP infinite conductivity pressure difference sensitivity

Figure 3.9 shows the cumulative production when HF-PDP is into the reservoir with with Infinite Conductive Fracture. In such plots, the higher the exponential decay for permeability in the hydraulic fracture, the lesser the cumulative production of the reservoir, especially the higher the exponent decay in the hydraulic permeability, the higher the decay especially going up from the factor $2.5 \cdot 10^{-3}$ represented on light grey.

30
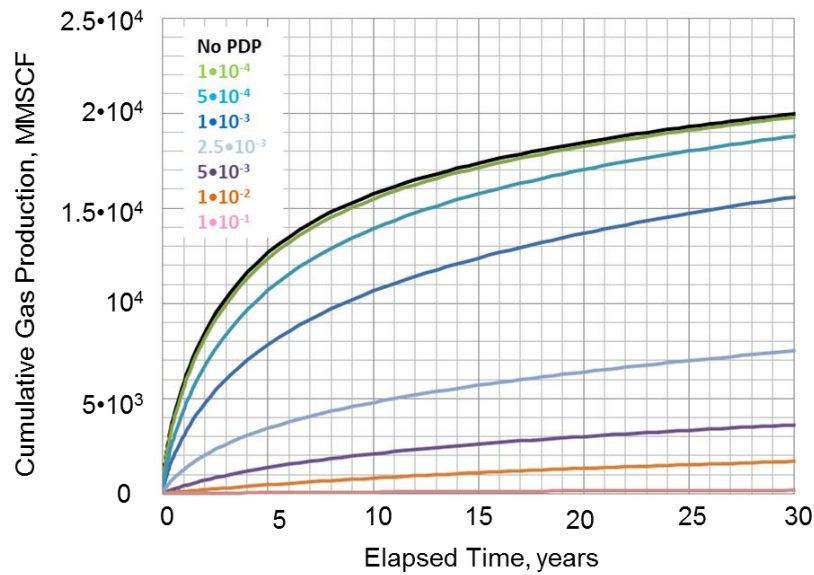
Figure 3.9: 30 year HF-PDP infinite conductivity production forecast

3.1.2.2 HF-PDP with Finite Conductive Fractures

This section focuses on the same case of the previous section, in this case considering finite fracture conductivity and using again the same parameters on table 3.1. Figure shows an immediate finite conductive flow regime as quarter slope in early time that manifests longer as higher exponent of permeability decay influences the production at constant pressure. Because the well is produced at constant pressure, the main effect is immediate conductivity lowering in the fractures to correspond to the permeability for the flowing pressure. In Figure 3.10, the transition from bilinear flow seen as ¼ slope to linear flow seen as ½ slope shortens as greater permeability decline exponent is introduced. Over time the fracture dimensionless conductivity losses influence as a result of loss in hydraulic fracture permeability as well as linear flow from the matrix dominates the flow of gas from the reservoir. Also, as figure previously showed, higher exponent factor above $5 \cdot 10^{-3}$ makes the RNP derivative to manifest a

31

valley of similar shape of a pseudo steady dual porosity which may represent the presence of an outside reservoir dominating the flow from the shale at longer times.
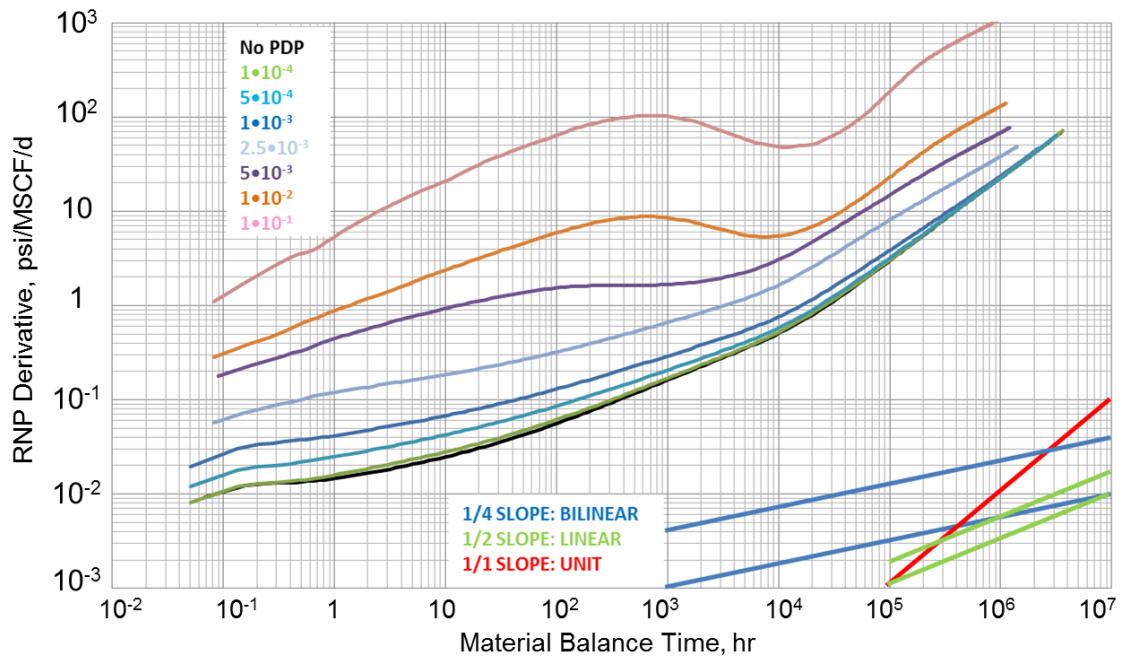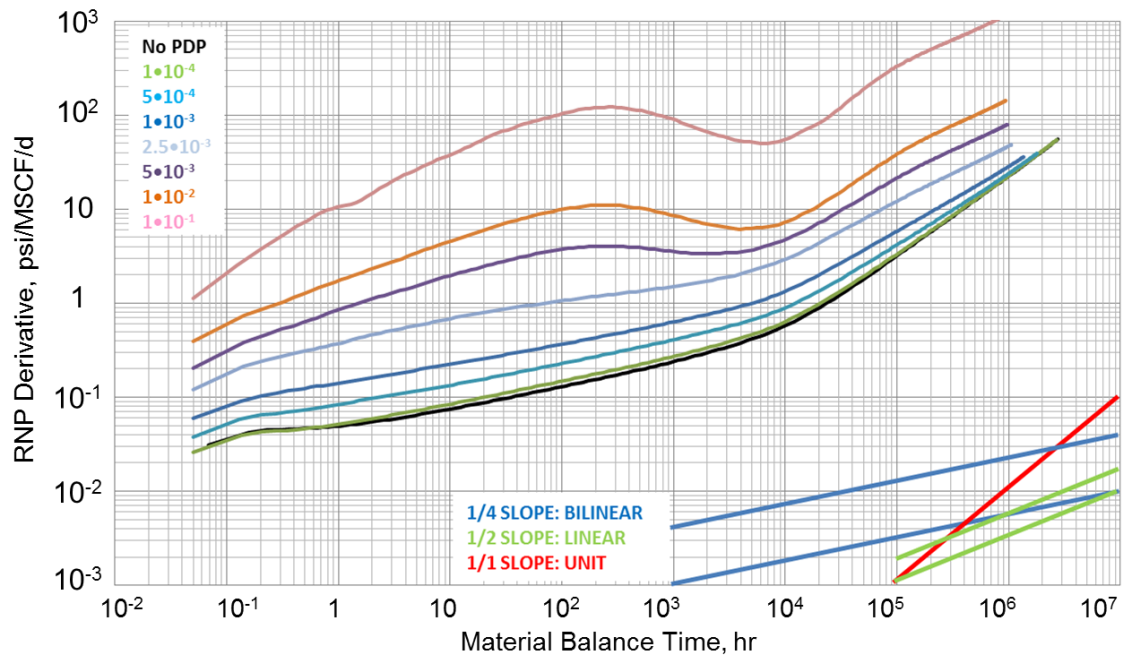

Figure 3.10: Increasing HF-PDP and finite conductivity (C_{fD}=10) sensitivity

As with Figure 3.7, HF-PDP with Finite Conductive Fracture is considered for sensitivity with the difference in flowing pressure at a fixed exponential factor of $1 \cdot 10^{-3}$. Figure 3.11 is different from other sensitive curves on difference in flowing pressure is the transition time. In this case the higher the pressure drops, the earlier the transition from bilinear to linear. One thing in common is the convergence towards unit slope
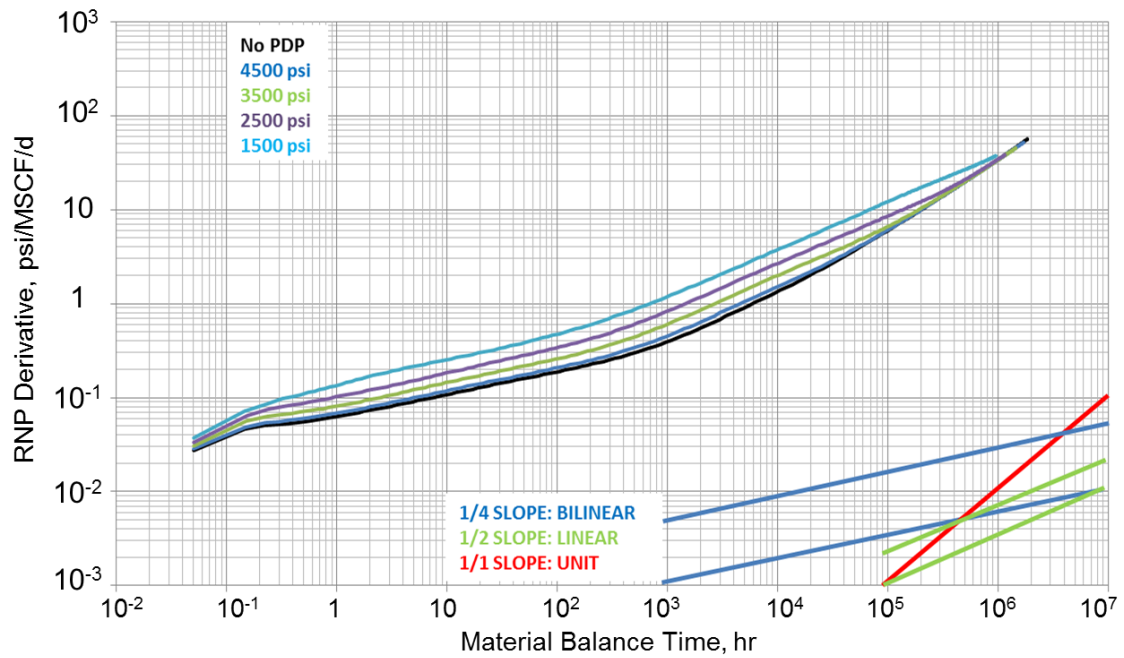
Figure 3.11: HF-PDP finite conductivity pressure difference sensitivity

Furthermore, well productivity index also decreases with permeability as the previous case of infinite conductive HF-PDP. The higher the exponent decay in the hydraulic permeability, the higher the decay, especially going up from the factor $2.5 \cdot 10^{-3}$ represented on light grey. Dramatic decay from factors of $1 \cdot 10^{-4}$ shows how big the difference between well performance is when finite conductive fractures influences production. Figure 3.12 shows this HF-PDP sensitivity of the production forecast.
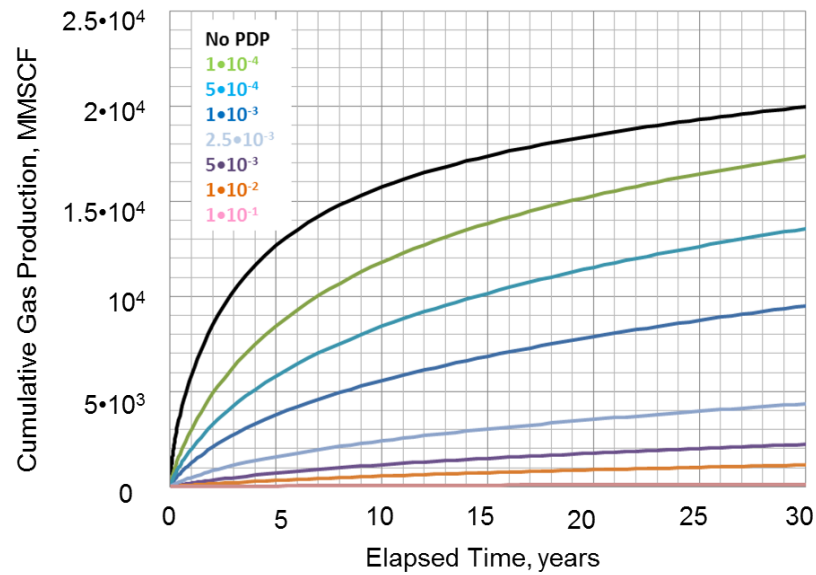
Figure 3.12: 30 year HF-PDP finite conductivity production forecast

3.2 Pressure Transient Sensitivity Analysis

Analyzing Pressure Transient data was not necessary because of the different behaviors each RNP showed on early time from matrix to hydraulic fracture pressure dependent permeability.

3.3 Reduced versus Exponential Declining Permeability

As previously investigated on later times, a final porous volume estimate can remain constant whether PDP is present or not in the matrix but a lower exponential decay values. For bigger values, unit slope that limits the volume takes longer to appear. It is evident that for bigger flowing pressures, the sooner an exponential decay achieves a constant permeability pore volume. It results interesting to see how close a constant reduced permeability can represent such phenomena when it is contrasted with the exponential permeability decay and as Figure 3.17 suggest, a reduction of 61% is experienced from a constant permeability behavior to an exponential one.

34
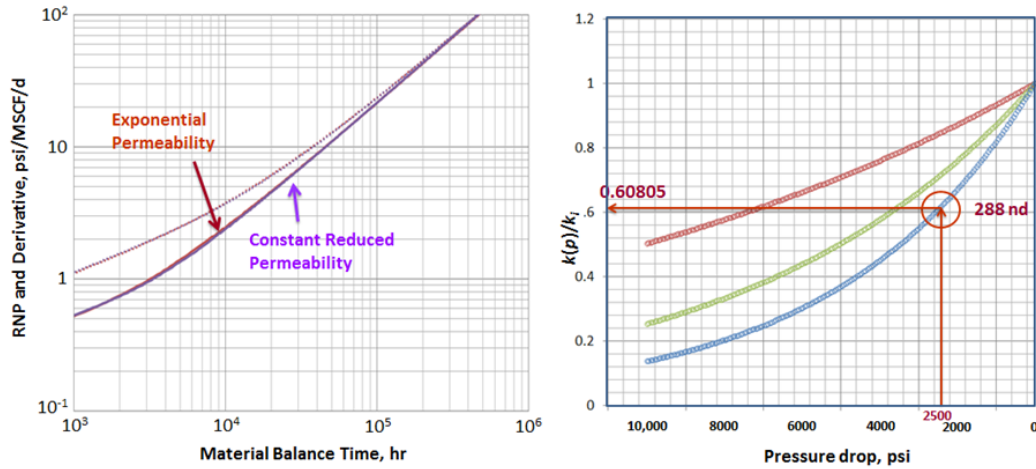
Figure 3.13: RNP at 2500 psia (left) and quantified reduction (right).

Contrasted with the exponential decay when forecast is set to 30 years, an error of 6% between the constant permeability case shown in brown and the exponential decay case, shown in green. Even with the case of a constant reduced permeability, the error is still not bigger than 6% as shown with the blue line. A curiosity we like to share on the right side of Figure 3.18 there is a big production separation at first five years. Between a constant reduced and an exponential decay case, the error is not bigger than 3% but when either case is compared with a constant permeability case, the error is more than 22%, making a constant permeability assumption so detrimental and sensitivity to our cumulative field production. It may work as explanation for why some reason some operators do not keep production of certain shales after 18 or 20 months, explaining further development and also may explain why additional fracture stimulation can provide deliverable production.

35
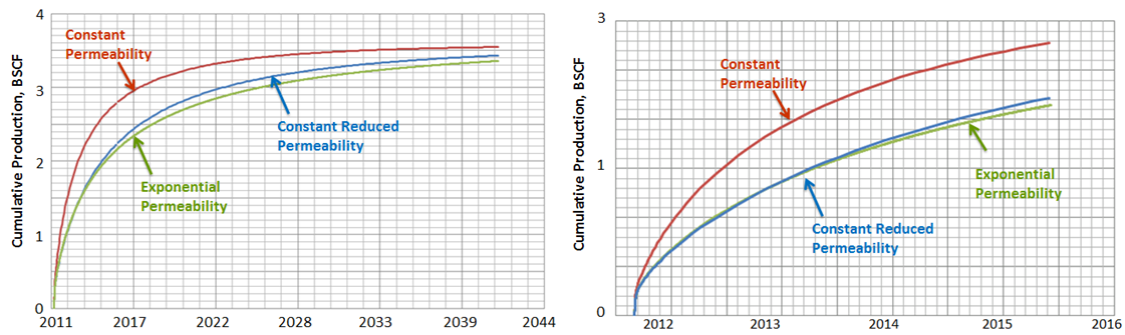
Figure 3.14: Production forecast comparison for 30 year and 5 year.

3.4 Chapter Summary

Sensitivity analysis on shale gas MTFHW shows different flow regime manifestations when they appear on log-log plots. Changes in matrix, hydraulic fracture and natural fracture permeability show difference response in production and pressure transient analysis.

In the analysis of Long Term Production Data, Matrix PDP usually shows changes in level of the pressure derivative as permeability increases or decreases. The lower the permeability makes also the sooner to appear the unit slope which declares the size of producing volume. When finite conductivity is present, sequential flow regime from bilinear-linear-unit is present and the previous signatures appear also on log-log plot.

Hydraulic Fracture PDP shows in the conductivity. The lesser the exponent decay on the fracture permeability, the lesser the conductivity and the higher the elevation of the derivative is raised but keeping the same unit slope level. It suggests the effect to transition towards PSS flow goes from linear flow towards bilinear as higher

36

factors of exponent decay enter in consideration. Also the more the decay in permeability in the hydraulic fracture, the longer the bilinear flow regime appears on time shortening the linear flow on the plot to the point that can hide from the pressure derivative of the RNP.

Having seen the production data analysis in the form of RNP, synthetic cases for build ups on these scenarios were not considered.

CHAPTER IV

FIELD CASES OF PRESSURE DEPENDENT PERMEABILITY

Chapter II briefly described pressure dependent permeability (PDP) in the matrix, and in hydraulic fractures. Chapter III showed sensitivity studies of PDP in shale reservoirs and showed that behavior of PDP matrix permeability is easily distinguished from DPD hydraulic fracture permeability on log-log diagnostic plots of RNP and its logarithmic derivative.

This chapter will show field cases of PDP from Fayetteville, Haynesville, and Horn River shale formations found in North America. For each hale, background information will be provided before showing field data illustrating distinct transient behavior. In particular, while the Fayetteville shale does not show apparent PDP behavior, Haynesville shale shows evidence of strong exponential permeability decline with increasing pressure difference, and Horn River shale shows slight increase in permeability with increasing pressure difference. The possibility of existing or created natural fractures in the formations is also considered.

4.1 Fayetteville Shale Case

Figure 4.1 illustrates that the Fayetteville shale is located at the state of Arkansas, near the Ouachita thrust front. Fayetteville shale gas wells produce ethane, propane and butane with a vitrinite reflectance of more than 1.5% (Zumberge et al. 2012).
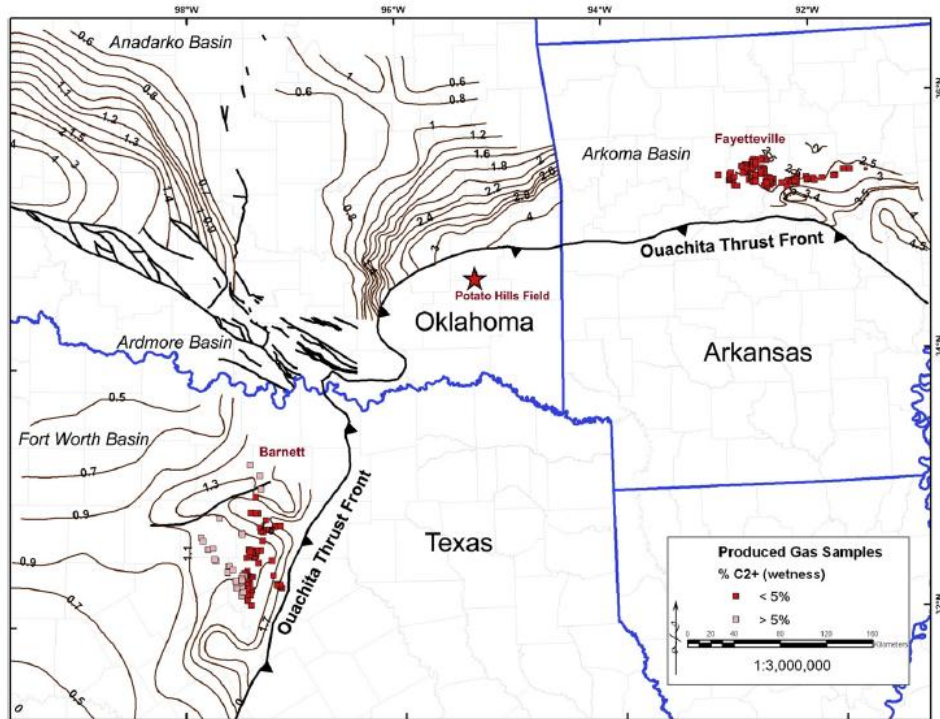
Figure 4.1: Location of Fayetteville shale

The size of the Fayetteville Shale is approximately 9000 square miles, and occurs at depths from 1000 to 7000 feet. The thickness of the Fayetteville Shale is from 20-200 feet. The shale is Mississippian age. Zumberge et al (2012) report that the average porosity is 0.08 and the effective shale matrix permeability is in the nanodarcies range.
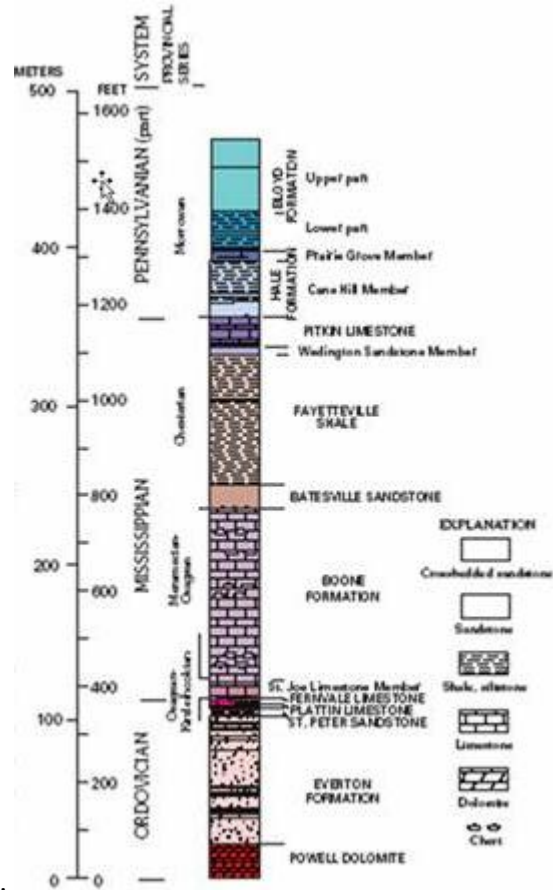
Figure 4.2: Stratigraphy of Fayetteville shale.

The well selected in this study has an approximate reservoir thickness of 322 ft. With a reservoir temperature of 125 $^\circ$F and TD at around 2,300 ft.MD and a with an initial reservoir pressure of 1050 psi.

On average, the wells were hydraulically fractured with a total of 43 perforation clusters along a 3400 ft average horizontal section length giving the average cluster spacing of about 80 ft. The wells are produced through 2-7/8" production tubing.

Available production data for the Fayetteville shale covers a period of almost two years. The data include surface casing and tubing pressure, and surface production rate (gas and water). The pressure and production data are collected on an approximately daily basis. Casing pressure is used to represent flowing bottomhole pressure by adding gas column static pressure to the measured surface casing pressure. Production and pressure history plots of a representative Fayetteville well appears in Figure 4.3.
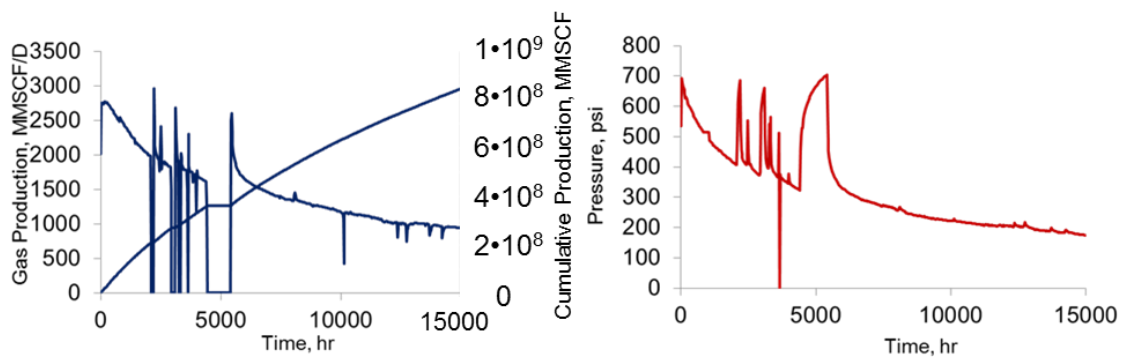
Figure 4.3: Fayetteville shale production and pressure history example

While it is not possible to estimate unique values for the shale permeability and fracture half-length, using the technique shown by Song and Ehlig-Economides (2011) a maximum value of 220 nd can be estimated for the shale permeability, which, in turn, gives a minimum value of 272 ft for the fracture half-length. Figure 4.4 shows RNP and derivative computed for the data in Figure 4.3 the late-time RNP behavior shows the ½ slope trend characteristic of linear flow.
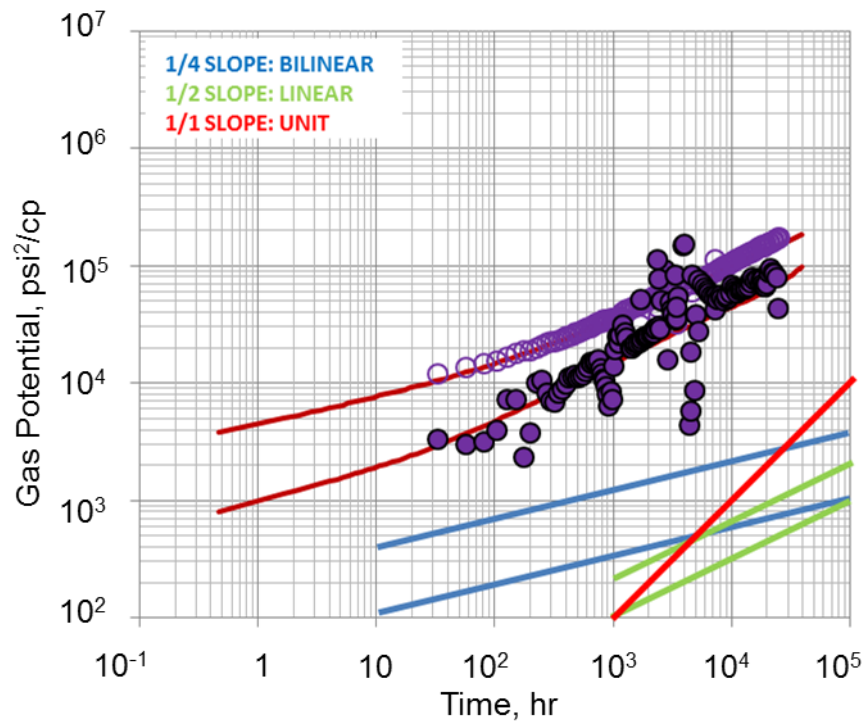
Figure 4.4: Fayetteville shale RNP match.

The data in Figure 4.3 include 2 buildup transients that are shown in Figure. 4.5.

Both show a ¼ slope trend suggesting finite conductivity hydraulic fractures.
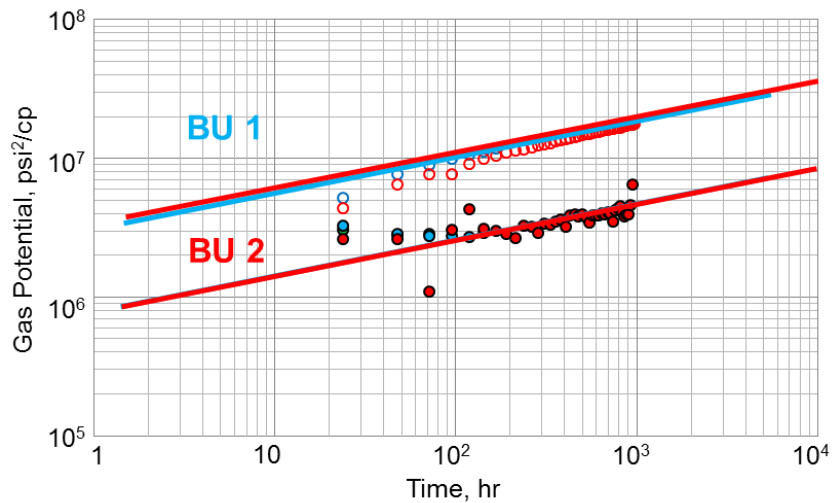
Figure 4.5: Fayetteville shale sequential build up

42

Table 4.1 shows calculations for fracture conductivity from Fig. 4.5 at each build up using the maximum permeability value previously used to estimate the fracture half-length. The buildup trends are nearly the same and provide an average conductivity of 3.7. Although the early behavior shows finite conductivity, the dimensionless conductivity is actually more than 200.

Table 4.1: Fayetteville conductivity values for each build up slope

	Time (hr)	k_fw (md-ft)	C_{fD}
BU 1	3000	3.83	217.12
BU 2	4500	3.69	209.46

Figure 4.6 shows a coupled BU-RNP to analyze different time frames of the reservoir behavior. BU pressure change and derivative have to be at same reference rate, q_{ref}, as used for the RNP. This is achieved by multiplying BU pressure change and derivative by q_{last}/q_{ref}. The model match shown in Fig.4.7 represents a Cartesian axes match. If and when longer term production data show evidence of unit slope trend in late time, the permeability and fracture half-length and conductivity data can be revised. This case shows the behavior when PDP behavior is lacking.
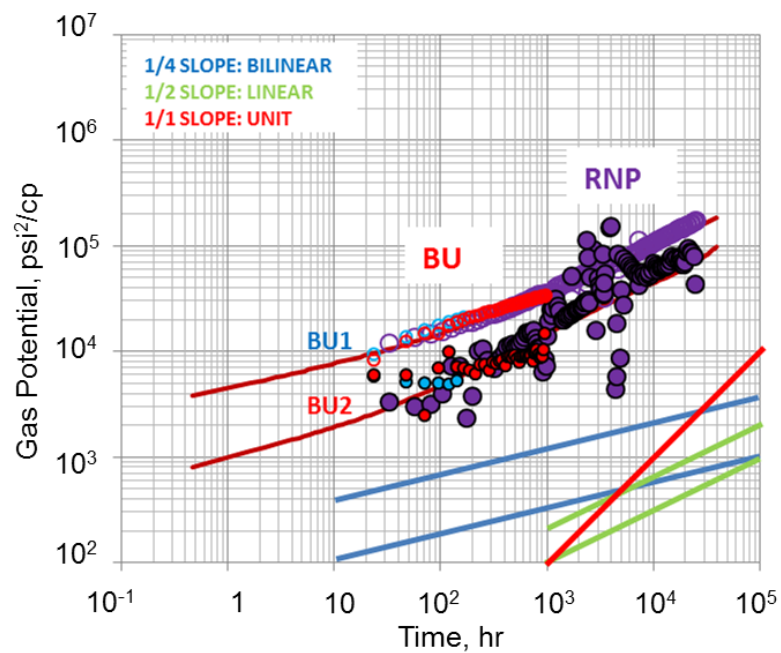
Figure 4.6: BU-RNP plot coupling last buildup and RNP response.
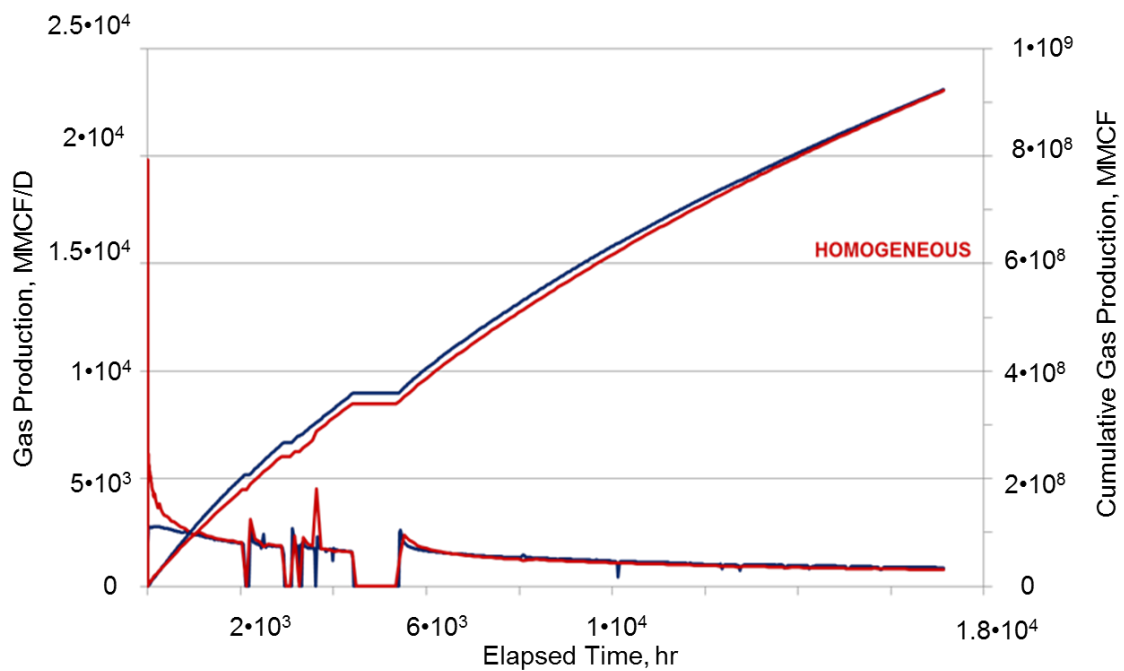
Figure 4.7: Cartesian match for Fayeteville shale

4.2 Haynesville Shale Case

The Haynesville shale, in East Texas and West Louisiana, below the Bossier formation, has evolved into one of the most prolific shale gas plays in North America, influenced by basement structures, local carbonate platforms and salt movement related to the opening of the Gulf of Mexico as represented on Fig. 4.8. One of the unique characteristics of the Haynesville Shale is that it is highly geopressured. The high pressure gradient tends to enhance porosity, gas content and apparent brittleness of shale gas reservoirs. It increases gas content through the increases in porosity and gas density. Although, intrinsically, the Haynesville Shale is not as brittle as the Barnett Shale of Fort Worth Basin, Texas, the near-fracture-gradient formation pressure makes the effective stress (lithostatic pressure minus pore pressure) of the Haynesville Shale very low and, thus, makes the formation easy to fracture.
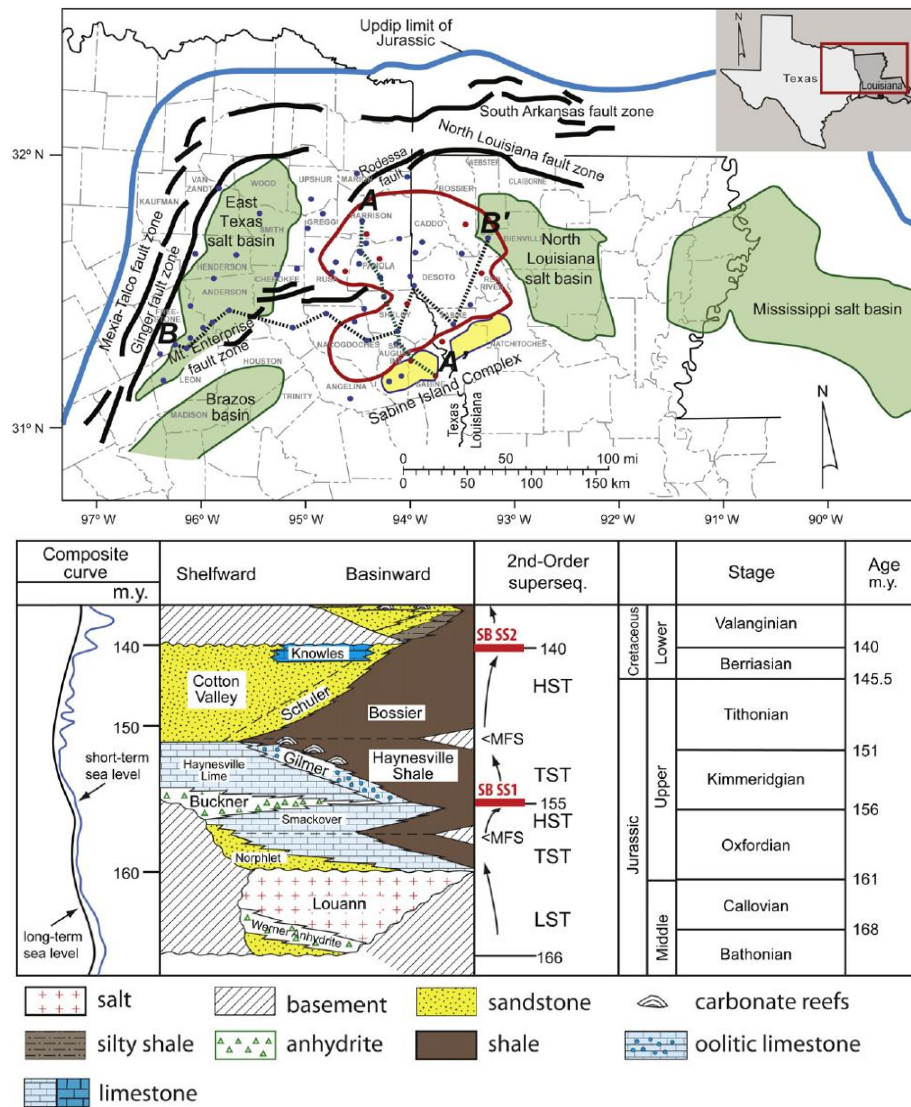
Figure 4.8: Haynesville shale location (above) and stratigraphy (below)

Hammes and Frébourg (2012) indicate that the Haynesville shale has high total organic content (TOC), good porosity, high gas saturation, low clay content and nanoDarcy permeability. Spatially, the Haynesville shale thins over pre-existing basement topography. There are three distinct types of natural fractures associated with

over-pressures or tectonics, namely pre-compaction, early digenetic and post-consolidation fractures.

Because of the extremely low permeability, static bottomhole pressures are difficult to determine, and shut-in tubing, shut-in casing or flowing casing pressures are normally reported in well tests. Bottomhole pressures of Haynesville Shale wells along with those of high-pressure wells of the Haynesville limestone and Bossier sand/shale were estimated from test data. Figure 4.9 represents pressure increases from 7,000 psi in Harrison County, Texas, to over 10,000 psi in San Augustine and Nacogdoches Counties, Texas, and Red River Parish, Louisiana. They are equivalent to pressure gradients from 0.6 psi to more than 0.95 psi/ft, with an average of 0.8 psi/ft (Wang and Hammes 2010)
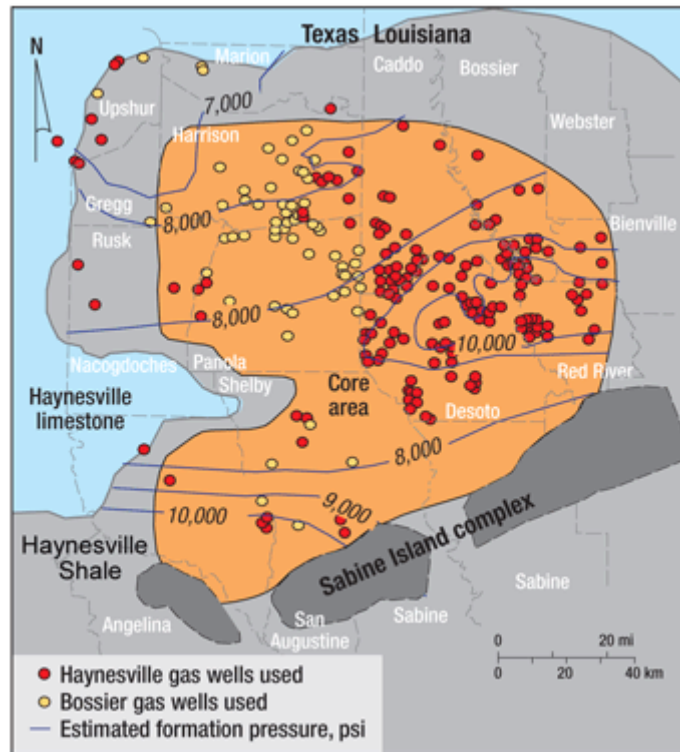
Figure 4.9: Pressure contours in the Haynesville shale

Younes et al. (2010) shows that the majority of fractures present in cores from this formation are carbonate filled and are not likely to contribute to production unless reopened during stimulation. Fig. 4.10 shows reactivated fractures that are typically limited to the vicinity of the stimulated fractures and do not extend far and the mechanically layered nature of the system poses its own challenge to play development because the less fractured layers are organic rich whereas the highly fractured layers are lean.
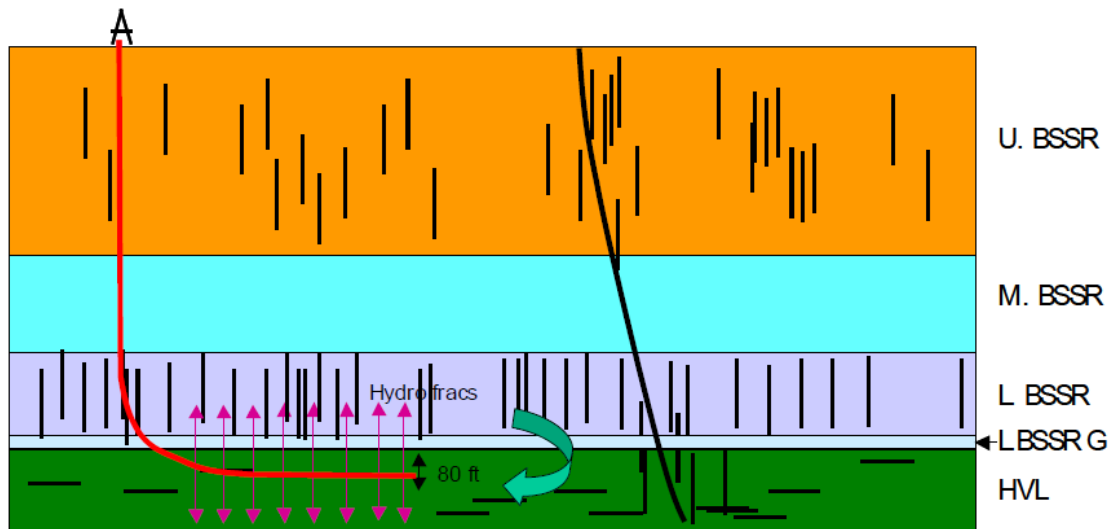
Figure 4.10: Geological representation of Haynesville

Our available data set of several wells located on Haynesville indicates an approximate TD around 12000 MD (15000 TVD) with approximate 17 stages of hydraulic fracturing stimulation that includes a total of 35 perforation clusters. Its fracture spacing ranges from 50 to 75 ft with an average value of 60 ft and hydraulic conductivity has been reported to range less than 10 md-ft in the case of chocked and crushed fracture.

Representative pressure and production rate data from Haynesville shale are shown in Fig. 4.11. The gauge data included permanent downhole gauge recording every 15 minutes, and gas production rate every hour. In this case there is no need to add the gas column static pressure because pressures are measured at bottom hole.
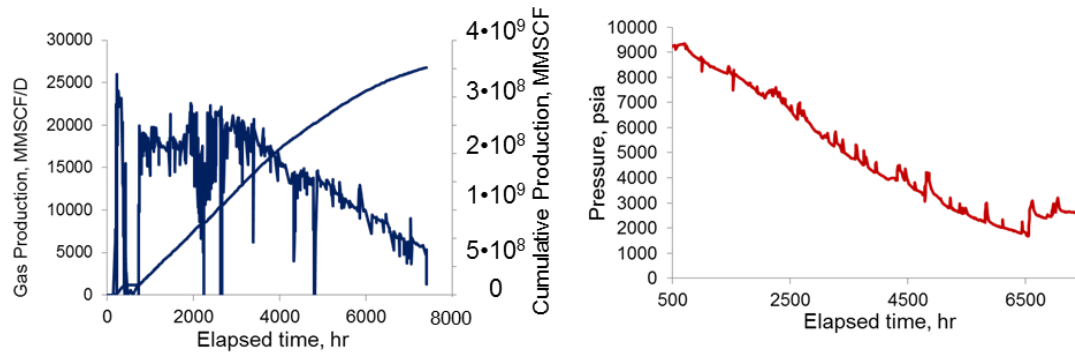
Figure 4.11: Haynesville shale production and pressure history example

Figure 4.12 shows the RNP and derivative response for this well. Early time shows a ¼ slope trend characteristic of bilinear flow, and late time behavior shows a unit slope. As shown by Song and Ehlig-Economides (2011), the unit slope defines the pore volume drained by the well. Assuming its extent is approximately defined by the extent of the fracture planes, the fracture area is estimated as 3125 ft^2.
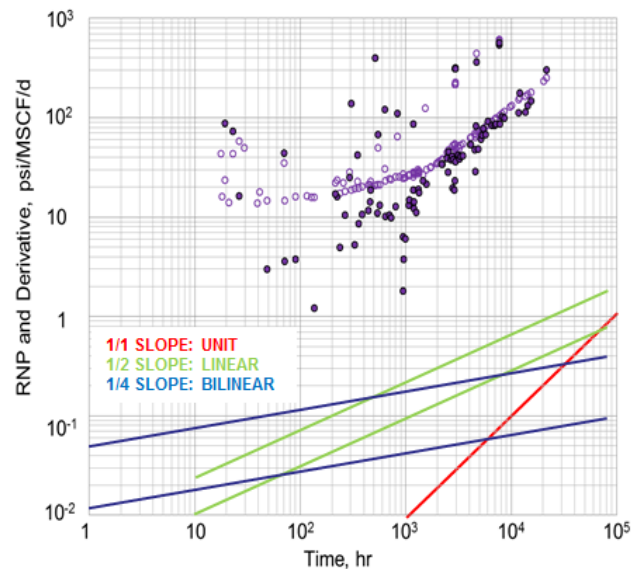
Figure 4.12: Haynesville RNP and derivative.

In turn, for a thickness of 150 ft, this corresponds to average fracture half-length of 115 ft. The end of linear flow behavior provides an estimate for the maximum possible permeability at the latest possible before the start of the pseudo-pseudo steady state of 257 nd and a minimum possible fracture conductivity value of 16 md-ft. The model match shown in the figure uses these parameter values. In overall, there is proper pressure measurement recognize several shut-in periods. First, a homogeneous model using the RNP shows a match with the infinite conductivity to the behavior of production. Figure 4.13 shows a fracture half-length of 115 ft and a boundary slope containing a SRV of 3.5 Tcf.
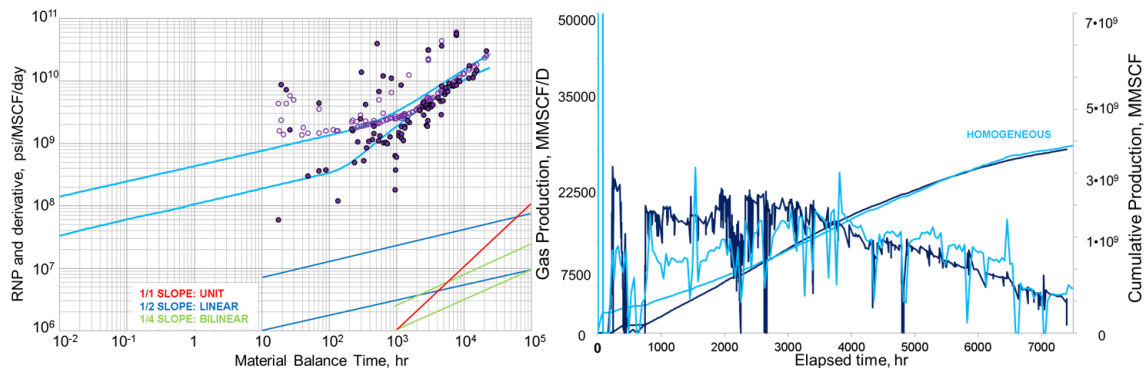
Figure 4.13: Haynesville RNP and cartesian match

Clarkson et al. (2011) suggested that successive build ups offer considerable insight about reservoir performance. This well offers several shut-ins for consideration and Figure 4.14 shows a log-log pressure and pressure derivative comparative diagnostic plot of three buildup (BU) transients from this well. Each buildup shows the ¼ slope

trend characteristic of finite conductive fractures, but each successive buildup is at a higher level, even after rate normalization. This means that either the shale effective permeability or that of the hydraulic fractures is decreasing in time.
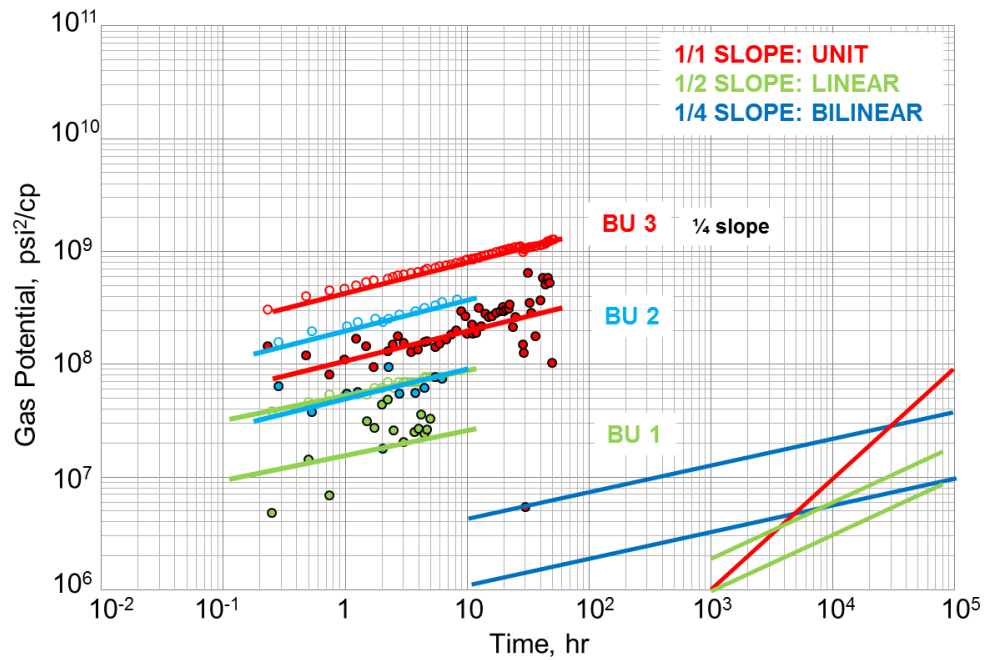
Figure 4.14: Haynesville sequential buildup.

Table 4.2 shows the calculations from Fig. 4.14 for each build up assuming the permeability value used for the match in Fig. 4.13. Figure 4.15 shows that the trend in fracture conductivity as a function of the decline in the model pressure can be modeled with an exponential function, which can be modeled as PDP for the hydraulic fracture permeability assuming a constant fracture width.

Table 4.2: Haynesville conductivity values for each build up slope

	Time (hr)	$k_f w$ (md-ft)	C_{fD}
BU 1	1436	21.75	162
BU 2	3260	1.93	14.7
BU 3	6500	0.3	2.77
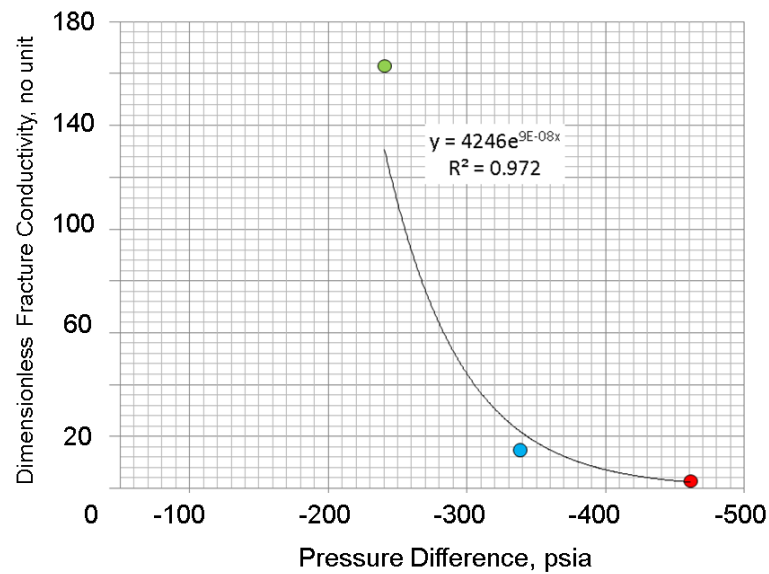
Figure 4.15: Haynesville conductivity exponential reduction.

Alternatively, the successive buildups can be interpreted with constant fracture conductivity and variable shale permeability. Table 4.3 shows permeability computed from each buildup assuming the fracture conductivity used for the match in Figure. 4.16.

Figure 4.20 shows an exponential function for the permeability behavior as a function of increasing pressure difference.
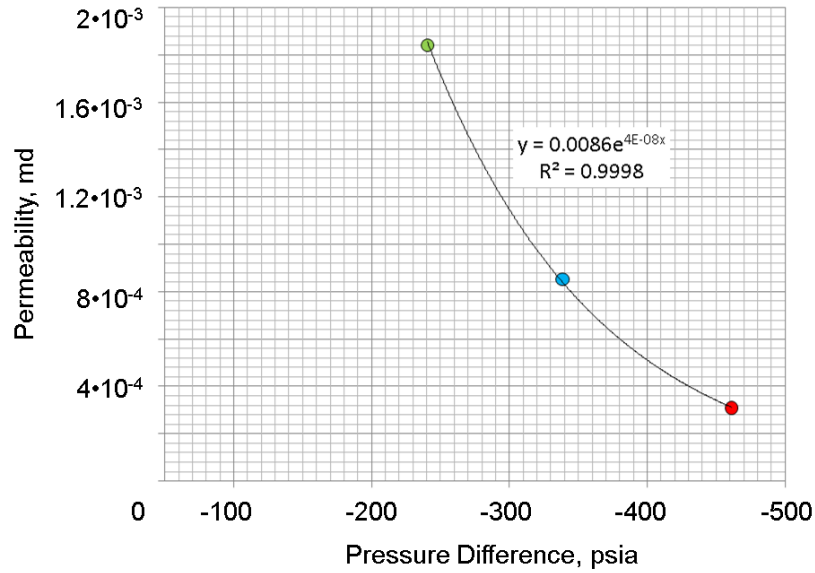
Figure 4.16: Haynesville permeability reduction.

This example shows two plausible scenarios, a reduction in conductivity and a reduction in permeability. Those changes can be captured by a changing well behavior modeling on Fig. 4.17, where either value of permeability or conductivity remains constant whereas the other experiments reduction.
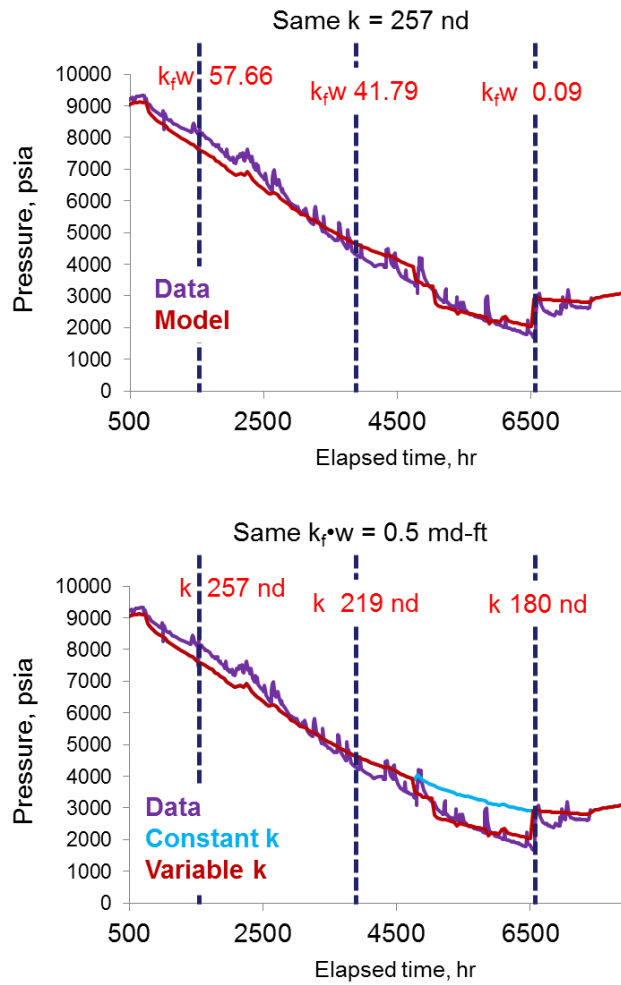
Figure 4.17: Haynesville changing well models.

Figure 4.18 combines the three buildups with the RNP and derivative graph. Each buildup is normalized by the ratio of q_{last}/q_{ref} as described previously. While a model match can be found for each BU-RNP combination, the important result is a match for the entire history that accounts for PDP in matrix or hydraulic fractures, or both. From sensitivity studies on early time performed on Chapter III, these sequential buildups shows a quarter slope that represents Figure 3.14, which is the case of a matrix

with pressure-dependent-permeability and strongly suggests the application of an exponential decay for permeability.
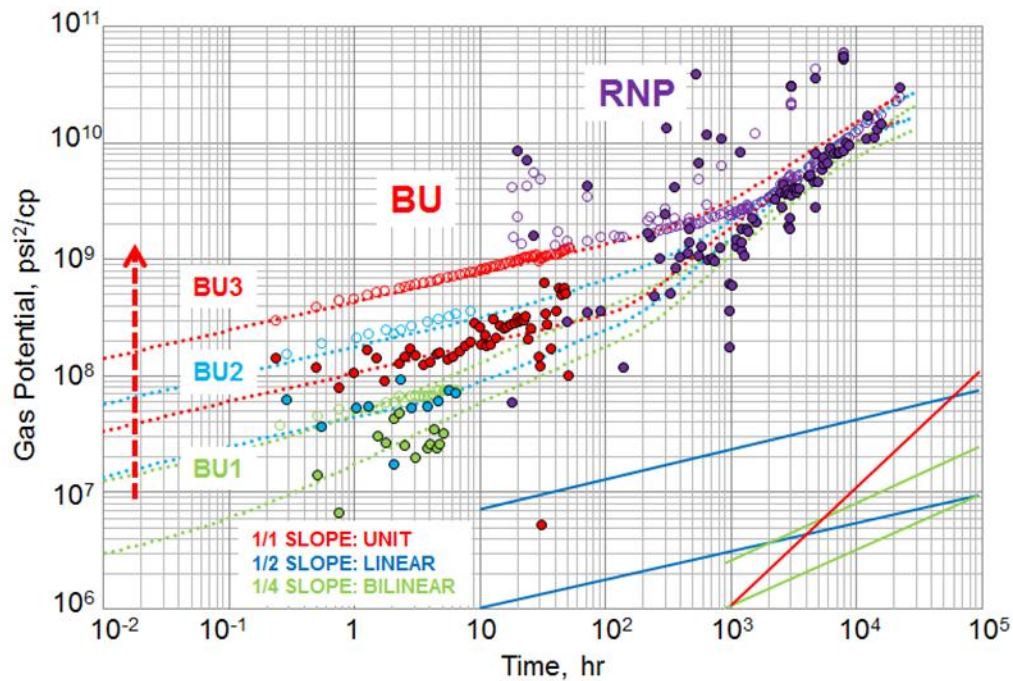
Figure 4.18: Haynesville normalized sequential BU-RNP

The Haynesville shale RNP response is unusual because it is dominated so early in time by unit slope, and hence behavior defining the drainage pore volume, so early in the production data. In many shale wells, unit slope behavior is not seen for years, but in Haynesville shale wells this behavior starts before one month on production.

Also on Figure 4.18, the bilinear flow regime shown on the BU overlain with the bilinear of the RNP confirming that they belong to the same flow regime in both analyses. That also means that any reduction of its flowing permeability does not come

from a pre-existing natural fracture but from a natural fracture network induced or reactivated during hydraulic fracturing.

Chapter III showed that orders of magnitude higher PDP exponents can induce behavior showing much lower apparent drainage pore volume. Figure 4.19 and 4.20 show a match for the observed behavior with a PDP exponent of $5 \cdot 10^{-4}$ and a fracture half-length of 175 ft in both RNP and production history, respectively.
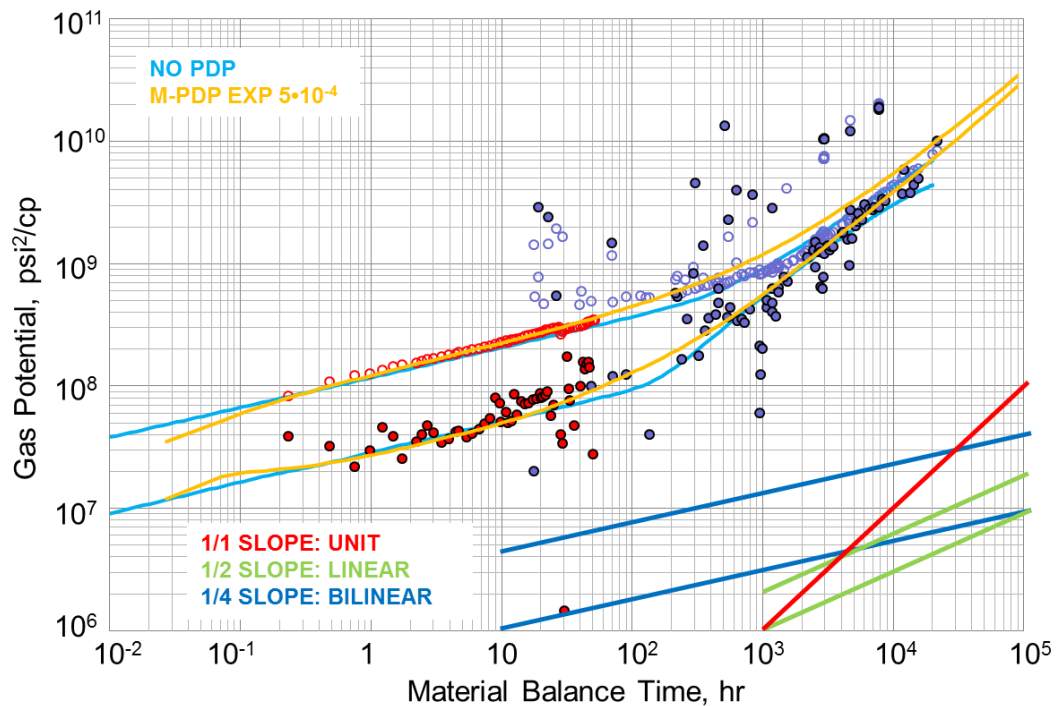
Figure 4.19: Haynesville Exponential decay permeability match.
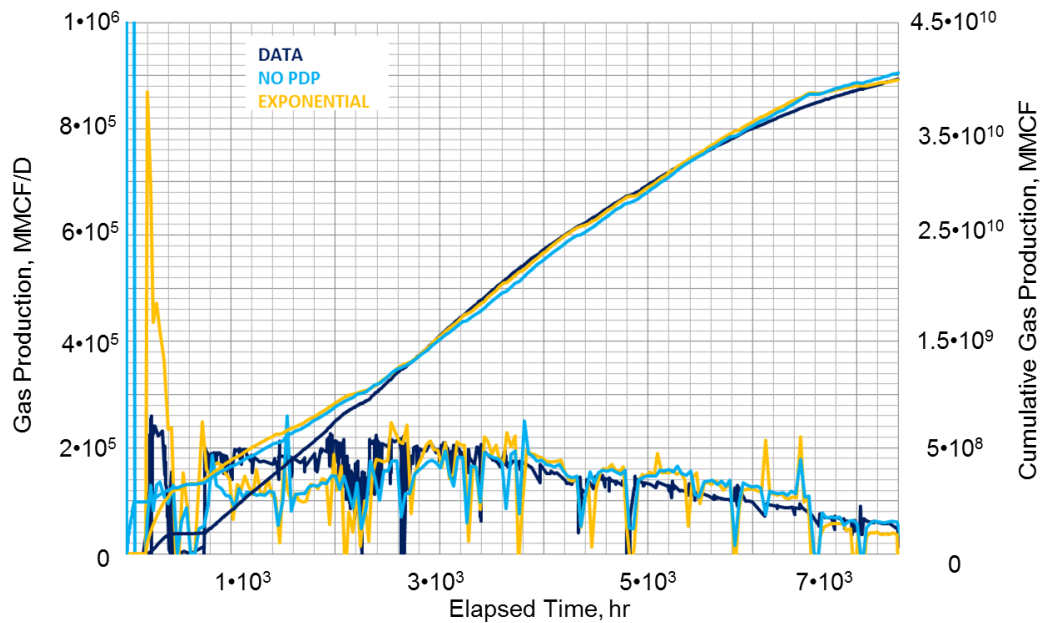
Figure 4.20: Haynesville History matching with exponential decay permeability

Once a production match satisfies the data, forecast should show how much this example can differ from homogeneous to M-PDP case. In Figure 4.21 the difference between these two models is more significant in the short term, translated in an error of 12% in the first 5 years and only 1.1% in the 30 year projection.
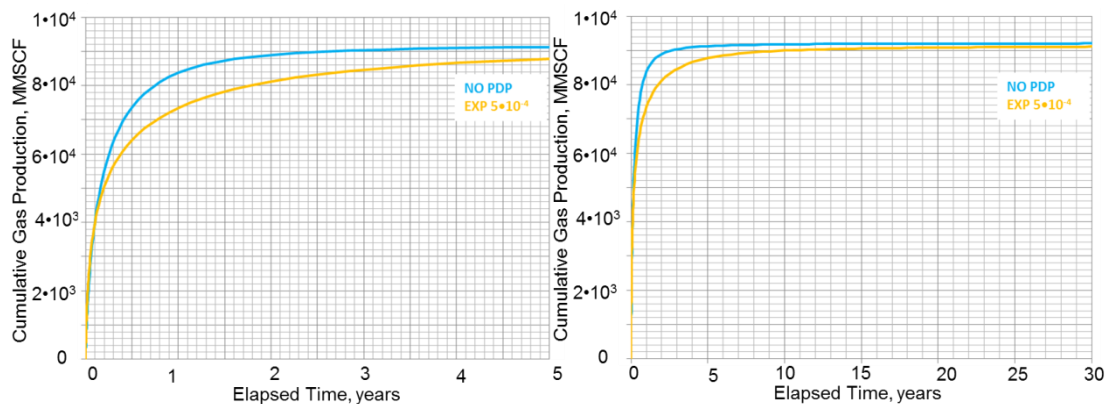
Figure 4.21: Production forecast with and without M-PDP.

4.3 Horn River Shale Case

The Horn River shale covers 3 million acres as the biggest resource of natural gas in a remote and difficult area located along the border between British Columbia and the North West territories, approximately 750 miles northwest of Edmonton, Alberta as Figure 4.22 illustrates.
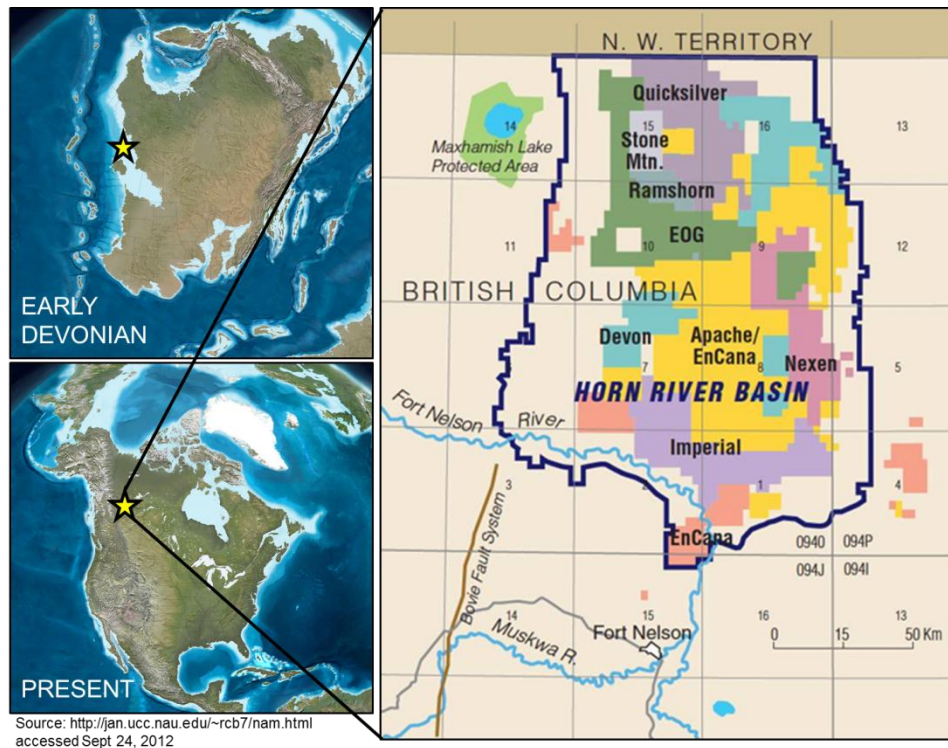
Figure 4.22: Leased acreage on Horn River.

This is of Upper Devonian age and comparable to the Barnett shale in aspects of depth, porosities, productivity, and shale qualities. However, it contains multiple potentially productive high temperature and over-pressured shale formations including the Carboniferous- Devonian Muskwa, Otter Park, Klua and Evie formations with an average temperature of 350°F and an initial pressure ranging from 5500 to 7250 psi for an

equivalent formation pressure gradient of 0.6-0.8 psi/ft. The average porosity in the Muskwa/Otterpark formation, shown in Figure 4.23, is 0.052 and the reported effective shale matrix permeability is in the nanodarcy range (Reynolds and Munn 2010).
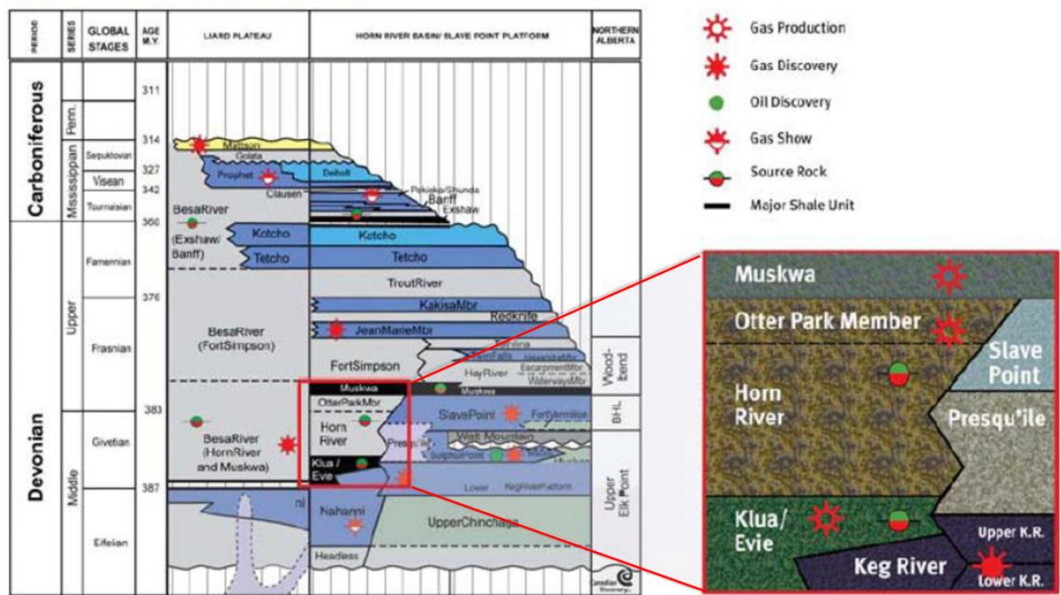
Figure 4.23: Geology of Horn River.

The well selected in this study is one of sixteen wells drilled from the same pad with average well spacing between adjacent wells of 880 ft. The well depths average about 9,000 ft TVD. Figure 4.24 shows the sixteen wells drilled from the same pad. The wells were put on production within a 3-month time span.
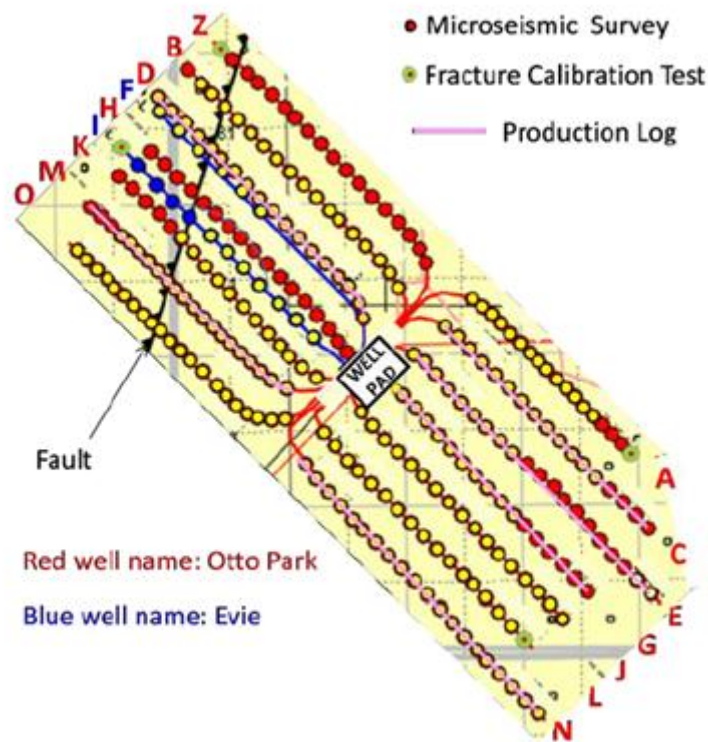
Figure 4.24: Well pad development for Horn River shale.

All the wells have at least one long shut-in period for 2-4 weeks started at the same time after around 5-6 months of production. On average, the wells were hydraulically fractured in 17 to 21 stages (18 on average) with a total of 25 to 45 perforation clusters (36 on average) along the 6380 ft average horizontal section length giving an average cluster spacing of about 165 ft. The wells are produced through 2-7/8" production tubing.

Available data for the Horn River shale covers a period of almost two years. The production data include surface casing and tubing pressure, and surface production rate (gas and water). The pressure and production data are collected on an approximately

daily basis. Casing pressure is used to represent flowing bottomhole pressure by adding gas column static pressure to the measured surface casing pressure. Production and pressure history plots of a representative Horn River well are shown in Figure 4.25.
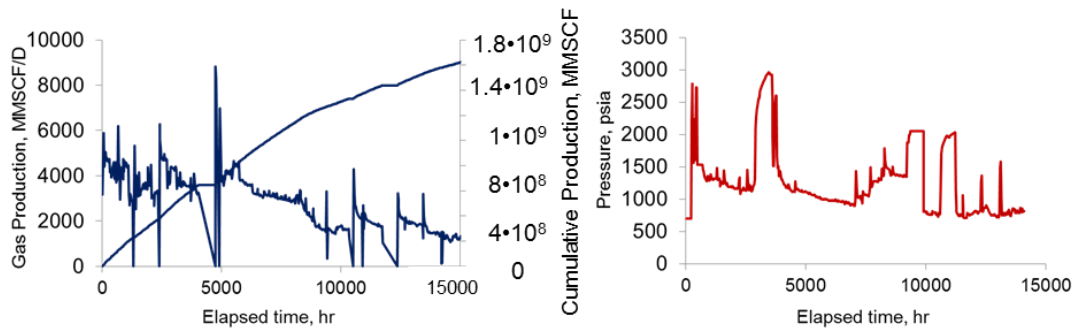
Figure 4.25: Horn River shale production and pressure history.

In this case, pressure measurement does not come from permanent downhole gauges but from wellhead casing and tubing records. Few buildups are found in the pressure history. Figure 4.26 shows the RNP and derivative diagnostic plot for a typical well. For these data the RNP derivative data tends to be quite scattered, and more emphasis must be put on use of the RNP data directly. The RNP trend is approximately ¼ slope behavior, and there is no indication of a turn toward a unit slope trend that could be used to quantify the well drainage pore volume. Knowing that the maximum effective fracture length is ½ the well spacing, the minimum permeability is estimated as 330 nd. In turn, a maximum estimate for the fracture conductivity based on the approximate ¼ slope is 1.8 md-ft. These values provide a reasonable model match for the RNP and Cartesian data shown in Figure 4.26.
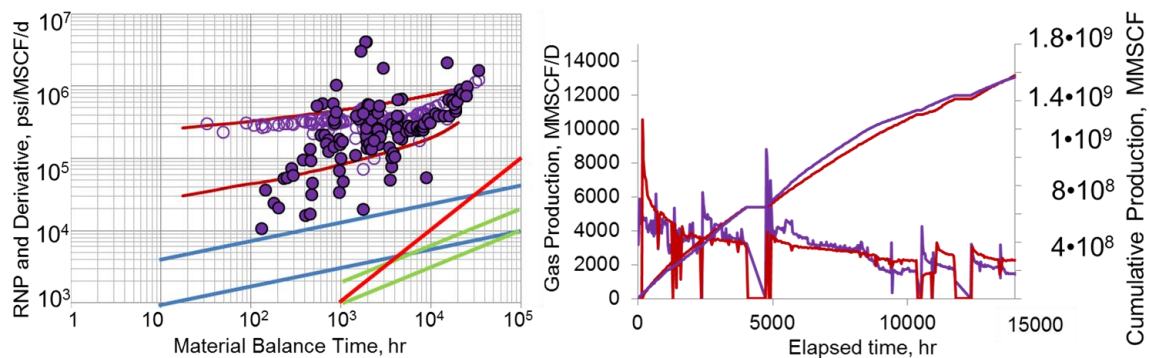
Figure 4.26: RNP and cartesian finite modeling match.

Sequential rate-normalized buildups (BU) in Figure 4.27 demonstrate once again a ¼ slope trend, but in this case the level drops in time, suggesting increasing permeability or fracture conductivity.
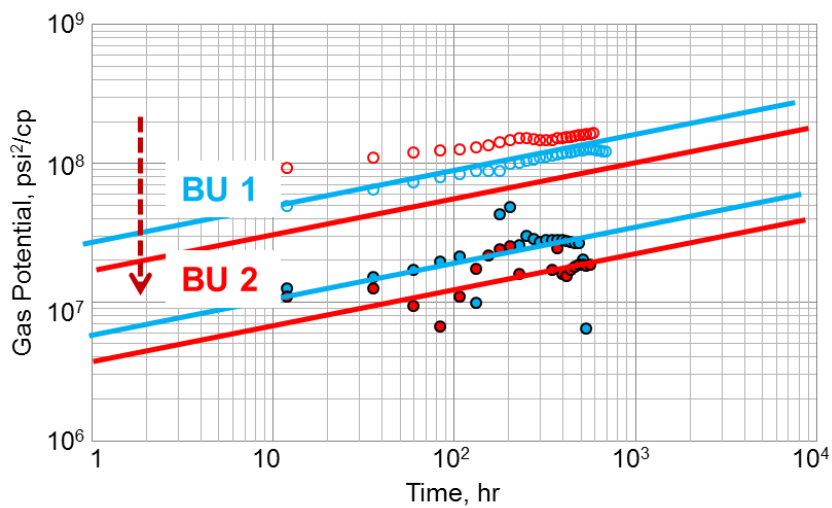
Figure 4.27: Horn River shale sequential buildup.

Table 4.3 and Figure 4.28 shows the fracture conductivity values calculated from Figure 4.27 at each build up using the permeability in the match shown in Figure. 4.26. From sensitivity studies on early time performed on Chapter III, these sequential buildups shows a quarter slope that represents Figure 4.30, which is the case of a matrix with pressure-dependent permeability but in this particular example, is an increase in the effective flowing permeability that can be modeled as a changing well model to capture it.

Table 4.3: Horn River conductivity values for each build up slope

	Time (hr)	k_fw (md-ft)	C_{fD}
BU 1	5000	0.5	32
BU 2	11000	1.8	117
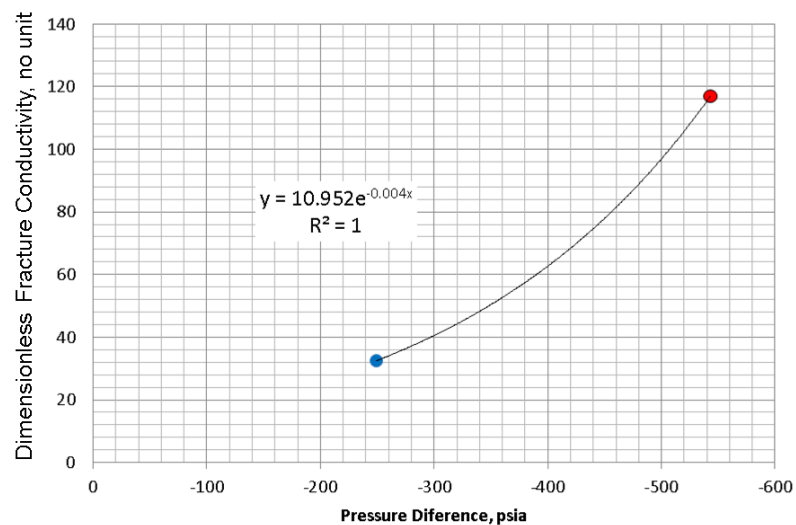
Figure 4.28: Horn River conductivity increase.

64

A different scenario is possible by matching the buildups to a specific permeability. Fig. 4.32 shows exponential fit for calculated values of permeability by keeping the same conductivity, inferring also a better match between the values and the behavior of this property in this particular reservoir.
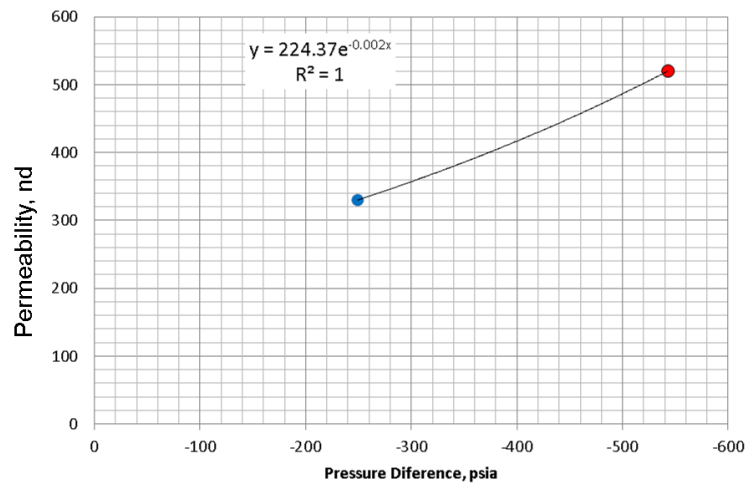
Figure 4.29: Horn River permeability increase.

This example shows two plausible scenarios, increasing conductivity or increasing permeability. Increasing permeability suggests the permeability used to match the data is an effective permeability of a natural fracture system with permeability increasing due to shear dilation as modeled by Tao, et al 2009 or alternatively this might be explained by increasing porosity and permeability as gas desorbed in the pore space (Shabro et al. 2012). Those changes are captured by changing well models shown in Fig. 4.30 where either value of permeability or conductivity remains constant while the other experiences reduction.
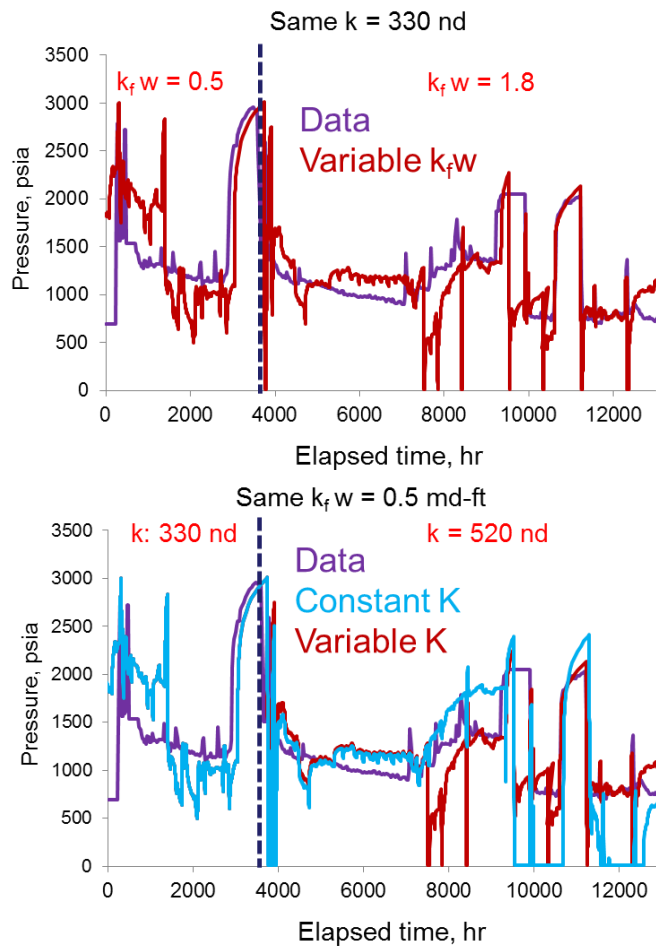
Figure 4.30: Horn River changing well models

As for the Haynesville example, the combined BU-RNP allows visualization of the dynamic behavior. Appiwathanasorn and Ehlig-Economides (2012) showed a dual porosity model matches for this well. Figure 4.31 includes the earlier buildup with high acquisition rate data, showing early time information for pressure transient analysis, and the second buildup shown previously. , along with dashed curves showing model matches for each buildup continuing through the long term production data shown in the RNP. The second buildup shown in red has considerably more apparent skin of 0.002

than the first buildup, and the RNP shows still higher apparent skin as previously mentioned. Also on Figure 4.31, the bilinear flow regime shown on the BU does not overlay the bilinear of the RNP strongly suggesting they don't belong to the same flow regime and the presence of a pre-existing natural fracture. That also means that any slight increase of its flowing permeability would correspond to an increase of the effective permeability of such pre-existing natural fracture network.
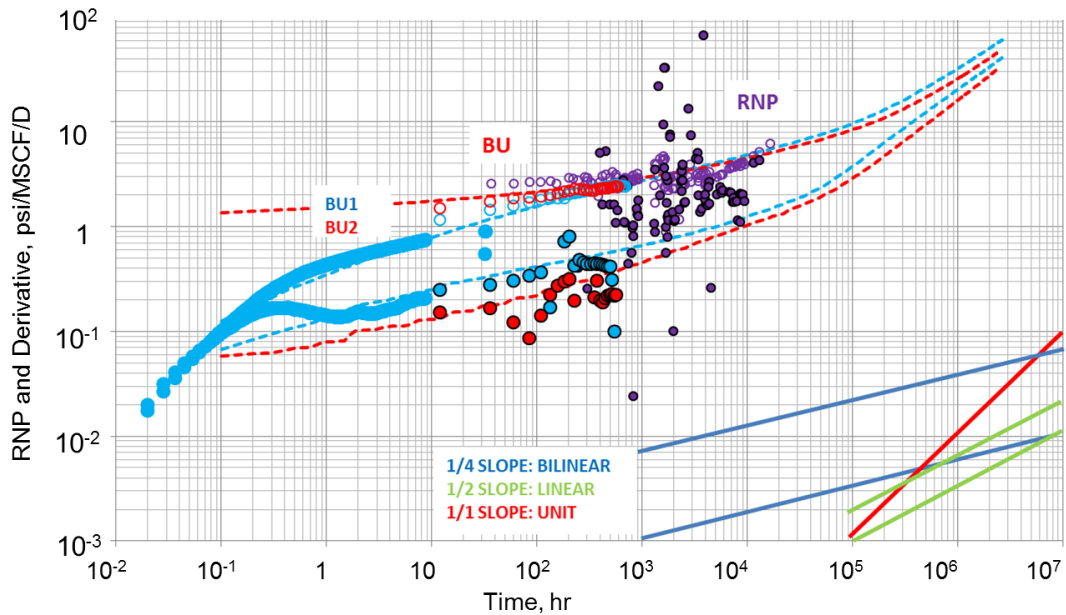
Figure 4.31: Horn River BU-RNP plot.

Once a production match satisfies the data, forecast should show how much this example can differ from the description that each build up offers in isolation. In Figure 4.32 the difference between these two models is more significant in the short term, translated in an error of 16% in the first 5 years and only 11% in the 30 year projection.
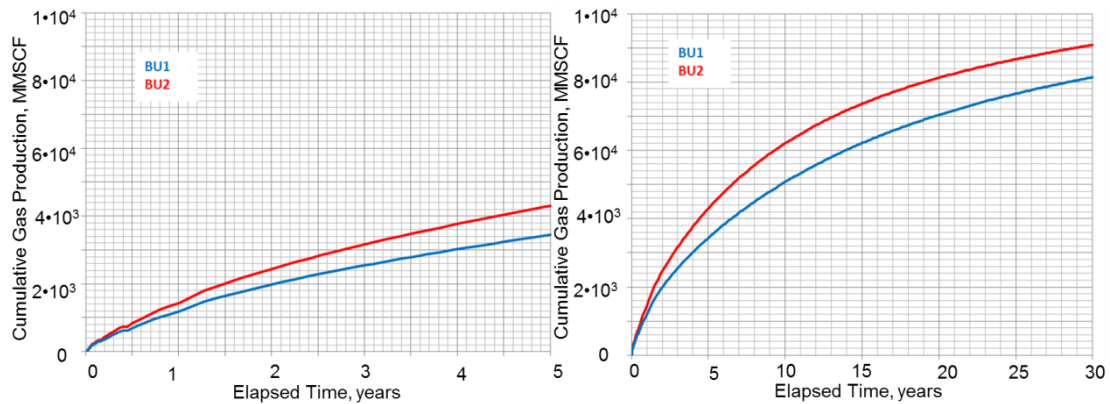
Figure 4.32: Horn River cumulative production forecast.

4.4 Chapter Summary

This chapter illustrated PDP behavior using data from Fayetteville, Haynesville and Fayetteville and Horn River shale wells. Possible interpretations include constant permeability for Fayetteville shale, exponential matrix permeability decay in Haynesville shale, and matrix permeability increase in Horn River shale.

While data may not fully confirm the evidence of pressure-dependent-permeability in all field cases, two scenarios with changing permeability or conductivity can match the data. Based on expected trends that synthetic data generates, all cases showed quarter slope in the pressure derivative response, suggesting a change in effective permeability with finite conductive fractures.

In the case of Fayetteville, most of the derivative responses were stable and kept the same level, inferring no change at all. This example showed a quarter slope in early time from the buildups that did not change on level at different drawdown times, strongly inferring that any substantial change in permeability is lacking.

Haynesville shale offered much better quality data for the analysis. The derivative levels rose with time indicating decay in the permeability. Two scenarios were modeled assuming the volume implied from late time boundary dominated flow was defined by the fracture half-length, and both provide a plausible result, each with a small permeability decline exponent. When more realistic fracture half-lengths are used the most likely answer is reduction in effective permeability, which may be related to a natural fracture induced during the hydraulic fracturing.

Horn River gave a different scenario. Producing wells are not isolated but gathered on a pad, with horizontal well spacing of 880 ft thus limiting the fracture half-length to a maximum of 440 ft. While they did not use a permanent downhole gauge, whenacquisition from wellhead data were acquired with a high data rate, this also enabled analysis of earlier time response trends. Pressure derivative showed quarter slope with a decreasing leveling over time, suggesting a rise in permeability or fracture conductivity. Modeling with increasing permeability matches satisfactory pressure response over production time. This insight suggests that existing effective permeability is enhanced by created natural fractures during production because of slow-slippage of the rock. Or, alternatively this might be explained by increasing porosity and permeability as gas is desorbed in the pore space

CHAPTER V

CONCLUSIONS AND RECOMMENDATIONS

The objective of this study was to confirm and quantify the evidence of pressure dependent permeability using pressure transient and production data analysis from shale formations like Haynesville, Fayetteville and Horn River.

This study focuses on sequential build up analysis at different drawdown times and the use of rate-normalized pressure (RNP). Derivative curves of both the buildup and RNP allow diagnosing the flow regimes and characterizing the behavior of the shale reservoir in the production life.

Sensitivity analysis on shale gas MTFHW shows different flow regime behavior on log-log plots, especially when changes in matrix or hydraulic fracture permeability are present.

This study shows the behavior between Haynesville, Fayetteville and Horn River are different from each other. While they all exhibit ¼ slope in early time, they differ from increasing, decreasing or stabilized levels of their pressure derivative responses at different drawdown times suggesting changes in effective permeability with finite conductivity fractures.

From the sequential analysis observed in Fayetteville, most of the derivative responses were stable and kept the same level, inferring no change at all. This example showed a ½ slope in RNP response and ¼ slope in early time from the buildups that did

not change on level at different drawdown times, strongly inferring that any substantial change in permeability is lacking.

Because permanent downhole gauges were used for pressure transient data generation, Haynesville shale offered much better quality data for the analysis. The derivative levels rose with time indicating decay in the permeability. Two scenarios were modeled assuming the volume implied from late time boundary dominated flow was defined by the fracture half-length, and both provide a plausible result, each with a small permeability decline exponent. When more realistic fracture half-lengths are used the most likely answer is reduction in effective permeability, which may be related to a natural fracture induced during the hydraulic fracturing. Horn River gave a different scenario. Producing wells are not isolated but gathered on a pad, with horizontal well spacing of 880 ft thus limiting the fracture half-length to a maximum of 440 ft. While they did not use a permanent downhole gauge, when acquisition from wellhead data were acquired with a high data rate, this also enabled analysis of earlier time response trends. Pressure derivative showed quarter slope with a decreasing leveling over time, suggesting a rise in permeability or fracture conductivity. Modeling with increasing permeability matches satisfactory pressure response over production time. This insight suggests that existing effective permeability is enhanced by created natural fractures during production because of slow-slippage of the rock. Or, alternatively this might be explained by increasing porosity and permeability as gas is desorbed in the pore space.

REFERENCES

Appiwathanasorn; and Ehlig-Economides, C.A. 2012. Evidence of Reopened Microfractures in Production Data Analysis of Hydraulically Fractured Shale Gas Wells. Paper presented at the SPE Canadian Unconventional Resources Conference, Calgary, Alberta, Canada. SPE 162842.

Clarkson, C.R., Jensen, J.L., and Blasingame, T. 2011. Reservoir Engineering for Unconventional Reservoirs: What Do We Have to Consider? Paper presented at the North American Unconventional Gas Conference and Exhibition, The Woodlands, Texas, USA. Society of Petroleum Engineers SPE-145080-MS. DOI: 10.2118/145080-ms.

Economides, M., Oligney, R., and Valkó, P. 2002. Unified Fracture Design (Hardbound) Orsa Press. *Houston, May*.

Ehlig-Economides, C.A., Martinez, H., and Okunola, D.S. 2009. Unified Pta and Pda Approach Enhances Well and Reservoir Characterization. Paper presented at the Latin American and Caribbean Petroleum Engineering Conference, Cartagena de Indias, Colombia. Society of Petroleum Engineers SPE-123042-MS. DOI: 10.2118/123042-ms.

Evers, J.F. and Soeiinah, E. 1977. Transient Tests and Long-Range Performance Predictions in Stress-Sensitive Gas Reservoirs. *SPE Journal of Petroleum Technology* **29** (08): 1025-1030. DOI: 10.2118/5423-PA

Franquet, B. 2004. Effect of Pressure-Dependent Permeability on Tight Gas Wells. Master of Science Thesis, Texas A&M University, College Station, Texas, USA.

Guenther, K.T., Perkins, D.S., Dale, B.A. et al. 2005. South Diana, Gulf of Mexico, U.S.A.: A Case Study in Reservoir Management of a Compacting Gas Reservoir. Paper presented at the International Petroleum Technology Conference, Doha, Qatar. International Petroleum Technology Conference IPTC-10900-MS. DOI: 10.2523/10900-ms.

Hammes, U. and Frébourg, G. 2012. Haynesville and Bossier Mudrocks: A Facies and Sequence Stratigraphic Investigation, East Texas and Louisiana, USA. *Marine and Petroleum Geology* **31** (1): 8-26. DOI: 10.1016/j.marpetgeo.2011.10.001

Kikani, J. and Pedrosa, O.a.J. 1991. Perturbation Analysis of Stress-Sensitive Reservoirs (Includes Associated Papers 25281 and 25292). *SPE Formation Evaluation* **6** (09): 379-386. DOI: 10.2118/20053-PA

Lorenz, J.C. 1999. Stress-Sensitive Reservoirs. *Journal of Petroleum Technology JPT*. DOI: 10.2118/50977-ms

Ostensen, R.W. 1986. The Effect of Stress-Dependent Permeability on Gas Production and Well Testing. *SPE Formation Evaluation* **1** (03): 227-235. DOI: 10.2118/11220-PA

Palacio, J.C. and Blasingame, T.A. 1993. *Decline-Curve Analysis with Type Curves – Analysis of Gas Well Production Data* Original edition. ISBN.

Pan, Y., Ewy, R.T., Ringe, D.P. et al. 2011. Pressure Transient and Production Data Analysis of Horizontal Well in Unconsolidated Formation in Frade, Brazil. Paper presented at the SPE Annual Technical Conference and Exhibition, Denver, Colorado, USA. SPE 147506. DOI: 10.2118/147506-MS.

Petro, D.R., Chu, W.-C., Burk, M.K. et al. 1997. Benefits of Pressure Transient Testing in Evaluating Compaction Effects: Gulf of Mexico Deepwater Turbidite Sands. Paper presented at the SPE Annual Technical Conference and Exhibition, San Antonio, Texas. 1997 Copyright 1997, Society of Petroleum Engineers, Inc. 00038938. DOI: 10.2118/38938-ms.

Reynolds, M.M. and Munn, D.L. 2010. Development Update for an Emerging Shale Gas Giant Field - Horn River Basin, British Columbia, Canada. Paper presented at the SPE Unconventional Gas Conference, Pittsburgh, Pennsylvania, USA. Society of Petroleum Engineers SPE-130103-MS. DOI: 10.2118/130103-ms.

Rodriguez, C.A. 2004. Stress-Dependent Permeability on Tight Gas Reservoirs. Master of Science Thesis, Texas A&M University, College Station, Texas, USA.

Samaniego V., F., Brigham, W.E., and Miller, F.G. 1977. An Investigation of Transient Flow of Reservoir Fluids Considering Pressure-Dependent Rock and Fluid Properties. *SPE Journal* **17** (04): 141-150. DOI: 10.2118/5593-PA

Shabro, V., Torres-Verdin, C., and Sepehrnoori, K. 2012. Forecasting Gas Production in Organic Shale with the Combined Numerical Simulation of Gas Diffusion in Kerogen, Langmuir Desorption from Kerogen Surfaces, and Advection in Nanopores. Paper presented at the SPE Annual Technical Conference and Exhibition, San Antonio, Texas, USA. Society of Petroleum Engineers SPE-159250-MS. DOI: 10.2118/159250-ms.

Song, B. and Ehlig-Economides, C.A. 2011. Rate-Normalized Pressure Analysis for Determination of Shale Gas Well Performance. Paper presented at the North American Unconventional Gas Conference and Exhibition, The Woodlands, Texas, USA. Society of Petroleum Engineers SPE-144031-MS. DOI: 10.2118/144031-ms.

Tao, Q., Ehlig-Economides, C.A., and Ghassemi, A. 2009. Investigation of Stress-Dependent Fracture Permeability in Naturally Fractured Reservoirs Using a Fully Coupled Poroelastic Displacement Discontinuity Model. Paper presented at the SPE Annual Technical Conference and Exhibition, New Orleans, Louisiana. Society of Petroleum Engineers SPE-124745-MS. DOI: 10.2118/124745-ms.

Vairogs, J. and Rhoades, V.W. 1973. Pressure Transient Tests in Formations Having Stress-Sensitive Permeability. *SPE Journal of Petroleum Technology* **25** (08): 965-970. DOI: 10.2118/4050-PA

Walsh, J.B. 1981. Effect of Pore Pressure and Confining Pressure on Fracture Permeability. *International Journal of Rock Mechanics and Mining Sciences & Geomechanics Abstracts* **18** (5): 429-435. DOI: 10.1016/0148-9062(81)90006-1

Wang, F.P. and Hammes, U. 2010. Effects of Petrophysical Factors on Haynesville Fluid Flow and Production. Paper presented at the AAPG Annual Convention and Exhibition, New Orleans- Louisiana. AAPG 752831.

Warpinski, N.R. 1991. Hydraulic Fracturing in Tight, Fissured Media. *SPE Journal of Petroleum Technology* **43** (2): 146-151, 208-209. DOI: 10.2118/20154-pa

Weaver, J.D., Rickman, R.D., and Luo, H. 2010. Fracture-Conductivity Loss Caused by Geochemical Interactions between Man-Made Proppants and Formations. *SPE Journal* **15** (1): pp. 116-124. DOI: 10.2118/118174-pa

Younes, A., Moore, H., Suumeyer, N. et al. 2010. Sweet Spotting the Haynesville-Bossier Shale Gas Play, Northwestern Louisiana, an Integrated Study. Paper presented at the AAPG Hedberg Conference, Austin, Texas. AAPG Search and Discovery Article #90122 (2010).

Zoback, M.D., Kohli, A., Das, I. et al. 2012. The Importance of Slow Slip on Faults During Hydraulic Fracturing Stimulation of Shale Gas Reservoirs. Paper presented at the SPE Americas Unconventional Resources Conference, Pittsburgh, Pennsylvania USA. Society of Petroleum Engineers SPE-155476-MS. DOI: 10.2118/155476-ms.

Zumberge, J., Ferworn, K., and Brown, S. 2012. Isotopic Reversal ('Rollover') in Shale Gases Produced from the Mississippian Barnett and Fayetteville Formations. *Marine and Petroleum Geology* **31** (1): 43-52. DOI: 10.1016

APPENDIX A

SINGLE POROSITY (HOMOGENEOUS) MODEL BEHAVIOR

The complete flow regimes for the single porosity model are shown in Song et al. (2011). However, only pseudolinear flow and pseudo pseudosteady state flow regime are likely to be seen in the shale gas field data since the shale matrix generally has very low permeability and the time required to reach compound linear flow regime or beyond is longer than the expected well life. Also, Song et al. (2011) generated the flow regimes using effectively infinite hydraulic fracture dimensionless conductivity (C_{fD}). In our work, however, the case with finite hydraulic fracture conductivity will also considered to capture the bilinear flow regime which can also be observed in field data. Cinco-Ley et al., 1978, indicated that the fracture conductivity is effectively finite when CfD is less than 300. This section will begin with the formation pseudolinear flow regime and later the formation to hydraulic fracture bilinear flow regime will be shown.

A.1.Formation Pseudolinear flow

The formation pseudolinear flow represents the flow from formation into hydraulic fracture plane before the boundary effect is sensed. During this period, each hydraulic fracture cluster is producing independently. The formation linear flow regime equation for shale gas flow from MTFHW is given by Eq. A.1 and A.2 in term of RNP and RNP', respectively.

$$RNP = \frac{40.93T}{n_F h x_F \sqrt{k}\left(\sqrt{\phi \mu c_t}\right)_i} \dots\dots\dots\dots\dots\dots\dots\dots\dots\dots\dots\dots\dots\dots\dots\dots\dots\dots (a.1)$$

$$RNP' = \frac{1}{2}\left[\frac{40.93T}{n_F h x_F \sqrt{k}\left(\sqrt{\phi \mu c_t}\right)_i}\sqrt{t}\right] \dots\dots\dots\dots\dots\dots\dots\dots\dots\dots\dots\dots\dots\dots\dots\dots\dots\dots(a.2)$$

Eq. a.1 and a.2 indicate that the formation pseudolinear flow regime will exhibit a 1/2 slope straight line for both RNP and RNP' on log-log plots versus material balance time. Also, it emphasizes that the RNP and RNP' always separate by factor of two (2).

The products of formation permeability and fracture half-length can be found from the log-log plots using Eq. a.1 or a.2. However, a.in general RNP' is more reliable because the RNP behavior may be affected by a fracture skin factor that alters the value of RNP. Figure A.2shows that the RNP' is independent of skin effect. Note that independent values for formation permeability and fracture half-length cannot be found because the linear flow relationship provides only one equation for these 2 unknowns.

A.2 Hydraulic Fractures - Matrix Bilinear flow

When hydraulic fractures have finite conductivity, the pressure drop along the fracture length cannot be neglected. In this case, bilinear flow will be observed in production and pressure data as a result of simultaneous linear flow in two perpendicular directions, i.e. flow inside hydraulic fracture and flow from the formation to the fracture plane. Cinco-Ley et al. (1978) demonstrated that infinite conductivity assumption is valid only when dimensionless fracture conductivity, $\left(k_f b_f\right)_D = \frac{k_f b_f}{k x_F}$, is less than 300. Otherwise the finite conductivity fracture model must be used.

Constant rate dimensionless solution for bilinear flow as presented by Cinco-Ley and Samaniego (1981) is shown in Eq. (a.3) while constant pressure dimensionless solutions as provided by Guppy et al. (1981) is shown in Eq. (a.4). *Constant rate*

$$p_{WD} = \frac{\pi}{\Gamma\left(\frac{5}{4}\right)\sqrt{2\left(k_f b_f\right)_D}} t_{DX_F}^{1/4}. \quad\text{...} \text{(a.3)}$$

Constant pressure

$$\frac{1}{Q_D} = \frac{\pi \Gamma\left(\frac{3}{4}\right)}{\sqrt{2\left(k_f b_f\right)_D}} t_{DX_F}^{1/4}. \quad\text{..}\text{(a.4)}$$

Where dimensionless variables for gas are defined by

$$p_{WD} = \frac{kh\left[m(p_i) - m(p_{wf})\right]}{1424qT}. \quad\text{...}\text{(a.5)}$$

$$t_{DX_F} = \frac{0.0002637kt}{(\phi\mu c_t)_i x_F^2}. \quad\text{...}\text{(a.6)}$$

$$\left(k_f b_f\right)_D = \frac{k_f b_f}{k x_F}. \quad\text{..}\text{(a.7)}$$

By comparing Eq. (a.3) with (a.4), it can be observed that the solutions for constant rate and constant pressure differ by factor of $\Gamma\left(\frac{3}{4}\right)/\Gamma\left(\frac{5}{4}\right)$ or 1.11 which indicates that the well producing at constant rate condition will encounter 1.1 times more pressure drop than when producing at constant pressure *during bilinear flow*. In section A.1 we saw that for linear flow the two solutions are separated by factor of $\frac{\pi}{2}$ or 1.57 times.

Substituting Eq. (a. 3) and (a.4) with definition of dimensionless variables defined by Eq. (a.5) thru (a.7), with modification by adding number of hydraulic fractures (nF) into the equation as to apply for multi-traverse fractured horizontal well, gives the dimensional equations for both constant rate and constant pressure condition as follows.

78

Constant rate

$$\Delta m(p) = \frac{444.75qT}{n_F\sqrt{k_F b_F}(\phi\mu c_t)^{1/4}k^{1/4}}\sqrt[4]{t} \quad \dots\dots\dots\dots\dots\dots\dots\dots\dots\dots\dots\dots\dots\dots\dots\dots\dots\dots(a.8)$$

Constant pressure

$$\frac{1}{q} = \frac{494\,\Delta m(p)T}{n_F h\sqrt{k_F b_F}(\phi\mu c_t)^{1/4}k^{1/4}}\sqrt[4]{t} \quad \dots\dots\dots\dots\dots\dots\dots\dots\dots\dots\dots\dots\dots\dots\dots\dots(a.9)$$

Next, differentiating Eq. (3.28) and (3.29) with respect to natural log of time to obtain pressure derivative solutions as follows:

Constant rate

$$\frac{\partial\Delta m(p)}{\partial\ln(t)} = \frac{1}{4}\left[\frac{444.75qT}{n_F\sqrt{k_F b_F}(\phi\mu c_t)^{1/4}k^{1/4}}\sqrt[4]{t}\right] \quad \dots\dots\dots\dots\dots\dots\dots\dots\dots\dots\dots\dots\dots(a.10)$$

Constant pressure

$$\frac{d\frac{1}{q}}{d\ln(t)} = \frac{1}{4}\left[\frac{494\Delta m(p)T}{n_F h\sqrt{k_F b_F}(\phi\mu c_t)^{1/4}k^{1/4}}\sqrt[4]{t}\right] \quad \dots\dots\dots\dots\dots\dots\dots\dots\dots\dots\dots\dots\dots(a.11)$$

Comparing Eq. (a.8) and (a.9) with (a.10) and (a.11) respectively indicates that pressure different and pressure derivative always separate by factor of four (4) during the *bilinear flow* period. Again, note that constant rate and constant pressure solutions for bilinear flow case s are separated by factor of 1.11.

Now, taking logarithmic both sides of Eq. (a.8) thru (a.11) gives bilinear flow solutions in log-log coordinate as follows:

Constant rate

$$log[\Delta m(p)] = \frac{1}{4}log(t) + log\left[\frac{444.75qT}{n_F\sqrt{k_F b_F}(\phi\mu c_t)^{1/4}k^{1/4}}\right] \quad \dots\dots\dots\dots\dots\dots\dots\dots\dots\dots(a.12)$$

and

$$log\left[\frac{\partial \Delta m(p)}{\partial \ln(t)}\right] = \frac{1}{4}log(t) + \frac{1}{4}log\left[\frac{444.75qT}{n_F\sqrt{k_F b_F}(\phi\mu c_t)^{1/4}k^{1/4}}\right] \dots \dots \dots \dots \dots \dots \dots \dots (\text{a.13})$$

Constant pressure

$$log\left(\frac{1}{q}\right) = \frac{1}{4}log(t) + log\left[\frac{444.75qT}{n_F\sqrt{k_F b_F}(\phi\mu c_t)^{1/4}k^{1/4}}\right] \dots \dots \dots \dots \dots \dots \dots (\text{a.14})$$

and

$$log\left[\frac{d\frac{1}{q}}{d\ln(t)}\right] = \frac{1}{4}log(t) + \frac{1}{4}log\left[\frac{494\Delta m(p)T}{n_F h\sqrt{k_F b_F}(\phi\mu c_t)^{1/4}k^{1/4}}\right] \dots \dots \dots \dots \dots \dots \dots (\text{a.15})$$

Again, these log-log form solutions emphasize that both pressure difference and pressure derivative will exhibit a quarter slope straight line on log-log pressure difference or pressure derivative versus time plot. Moreover, this confirms that the value of the pressure difference will always be higher than of pressure derivative by 4 times during bilinear flow regardless of at which condition the well is producing, provided there is no fracture skin. As for linear flow, when there is fracture skin, the derivative response will show ¼ slope even if the pressure difference does not.

Though the condition is not likely, the single porosity model may be used to represent a dual porosity formation characterized with primary porosity of the shale matrix and secondary porosity as a fracture network if the difference in conductivity between the media is small. In this case, the flow from the matrix may not only flow into the reopened fracture network, but will also enter directly into the hydraulic fractures. This condition could be considered as simultaneous flows from multiple layers with different permeabilities into the well, and the single porosity model might work fine but

the "average" or "effective" permeability must be used instead of the absolute matrix permeability to represent the average properties of the formations and fracture network.

Also, the single porosity model may be adjusted to represent the flow from the shale matrix into the fracture network by considering that parameters previously related to hydraulic fracture as applying instead to the fracture network.

APPENDIX B

DIAGNOSIS USING RNP AND ITS DERIVATIVE

The actual production data is never limited to just constant rate, or constant pressure behavior, it is useful to be able to use only one model to characterize both behaviors. The concept of using superposition time function instead of the actual time has been introduced. The material balance time (t_e) is one of superposition time functions which is defined as cumulative production divided by instantaneous rate, or

$$t_e = \frac{Q}{q}$$ ....(b.1)

Blasingame et al. (1991) and Agarwal et al. (1998) have shown that when the material balance time can be used instead of actual time rate-normalized pressure (RNP) behaves like the drawdown pressure resulting from constant rate production. They showed that the concept accurately represents the boundary dominated flow regime. However, for this study we need to evaluate whether the RNP processing of rate decline during constant pressure production produces the same behavior as would occur by modeling drawdown under constant rate production for the linear and bilinear flow regimes.

B.1 Bilinear flow

First, the constant rate and constant pressure equations are shown in equations (b.1) and (b.2), respectively.

$$p_{WD} = \frac{\pi}{\Gamma(\frac{5}{4})\sqrt{2(k_f b_f)_D}} t_{D_{XF,r}}^{1/4} \quad \text{...(b.2)}$$

$$\frac{1}{Q_D} = \frac{\pi\Gamma(\frac{3}{4})}{\sqrt{2(k_f b_f)_D}} t_{D_{XF,p}}^{1/4} \quad \text{..(b.3)}$$

Where and are the dimensionless time function for constant rate and constant pressure conditions, respectively.

First, equating Eq. (b.2) and (b.3) to find the relation between two time functions when P_{WD} = 1/q_D:

$$\frac{\pi}{\Gamma(\frac{5}{4})\sqrt{2(k_f b_f)_D}} t_{D_{XF,r}}^{1/4} = \frac{\pi\Gamma(\frac{3}{4})}{\sqrt{2(k_f b_f)_D}} t_{D_{XF,p}}^{1/4} \quad \text{...................................(b.4)}$$

Cancelling terms in Eq. (b.4) to have:

$$\frac{1}{\Gamma(\frac{5}{4})} t_{D_{XF,r}}^{1/4} = \Gamma(\frac{3}{4}) t_{D_{XF,p}}^{1/4} \quad \text{...(b.5)}$$

Adjusting the form and solve for in terms of :

$$t_{D_{XF,r}}^{1/4} = \Gamma\left(\frac{5}{4}\right) . \Gamma(\frac{3}{4}) t_{D_{XF,p}}^{1/4} \quad \text{.......................................(b.6)}$$

Since $\Gamma\left(\frac{5}{4}\right)$=0.9064 and $\Gamma(\frac{3}{4})$=1.2254 . Therefore, Eq. (d.6) can be rewritten as:

$$t_{D_{XF,r}} = 1.52 t_{D_{XF,p}} \quad \text{..(b.7)}$$

Equation (b.7) indicates that constant rate time function will be larger than constant pressure function by 1.52 times during bilinear flow regime.

Now, let's find material balance time function for bilinear flow regime that converts constant pressure to virtual constant rate:

Rearranging Eq. (b.3) for flow rate, we have

83

$$q_D = \frac{\sqrt{2(k_f b_f)_D}}{\pi \Gamma(\frac{3}{4}) t_{DX_{F,p}}^{1/4}} \quad\text{...(b.8)}$$

Integrating Eq. (b.8) respect to time to get cumulative production equation:

$$Q_D = \int q_D dt_{DX_{F,p}} = \frac{4}{3} \frac{\sqrt{2(k_f b_f)_D}}{\pi \Gamma(\frac{3}{4})} t_{DX_{F,p}}^{3/4} \quad\text{...............................(b.9)}$$

Dividing Eq. (b.9) with Eq. (b.8) to get a material balance time function, in terms of :

$$t_{eD,p} = \frac{Q_D}{q_d} = \frac{4}{3} t_{DX_{F,p}} \quad\text{...(b.10)}$$

Equation (b.10) indicates that the RNP and RNP' diagnostic plots using material balance time function will shift the plots the right (later) by factor of (4/3) or 1.33 times during bilinear flow regime.

Rearranging Eq. (b.10), we know that

$$t_{DX_{F,p}} = \frac{3}{4} t_{eD,p} \quad\text{...(b.11)}$$

Substituting Eq. (b.11) into (b.7) to get

$$t_{DX_{F,r}} = 1.522 \left[\frac{3}{4} t_{eD,p}\right] \quad\text{..(b.12)}$$

Finalize Eq. (b.12), we have

$$t_{DX_{F,r}} = 1.14 t_{eD,p} \quad\text{...(b.13)}$$

Therefore, the constant rate time function will be larger than the material balance time function by a factor of 1.14 during bilinear flow regime.

Comparing Eq. (b.13) with (b.7), it appears that material balance time function will shift constant pressure plots to be closer to constant rate plots, but still not identical. This implies that when plotting RNP and RNP derivative by using material balance time

function, a multiplier correction factor of 1.14 is required to convert completely the constant pressure plots to the constant rate plots.

D.2 Linear flow

The observations for linear flow have been presented by Anderson and Mattar (2003). The same methodology as shown for the bilinear flow is used. The results are recapped here for completeness.

First, the constant rate and constant pressure equations for linear flow regime are shown in Eq. (b.14) and (b.15), respectively.

$$p_{WD} = \sqrt{\pi t_{D,r}} \quad \text{..(b.14)}$$

$$\frac{1}{q_D} = \frac{\pi}{2}\sqrt{\pi t_{D,p}} \quad \text{.. (b.15)}$$

Where and are the dimensionless time function for constant rate and constant pressure conditions, respectively.

Now, equating Eq. (b.14) and (b.15) to find the relation between two time functions when $P_{wD} = 1/q_D$, we have:

$$\sqrt{\pi t_{D,r}} = \frac{\pi}{2}\sqrt{\pi t_{D,p}} \quad \text{...(b.16)}$$

Cancelling terms in Eq. (d.16) to have:

$$\sqrt{t_{D,r}} = \frac{\pi}{2}\sqrt{t_{D,p}} \quad \text{..(b.17)}$$

Adjusting the form and solve for in terms of:

$$t_{D,r} = \frac{\pi^2}{2}t_{D,p} = 2.46t_{D,p} \quad \text{.. (b.18)}$$

Equation (b.18) indicates that constant rate time function will be larger than constant pressure function by 2.46 times during linear flow regime.

Now, let's find material balance time function for linear flow regime that converts constant pressure to virtual constant rate.

Rearranging Eq. (b.15) for flow rate, we have

$$q_D = \frac{2}{\pi\sqrt{\pi t_{D,p}}} \quad\text{...(b.19)}$$

Integrating Eq. (b.19) respect to time to get cumulative production equation:

$$Q_D = \int q_D dt_{D_{X_{F,p}}} = 2\left[\frac{2}{\pi\sqrt{\pi}}\right] t_{D,p}^{1/2} \quad\text{...(b.20)}$$

Dividing Eq. (b.20) with Eq. (b.19) to get a material balance time function, $t_{eD,p}$, in terms of $t_{D,p}$:

$$t_{eD,p} = 2t_{D,p} \quad\text{..(b.21)}$$

Equation (b.21) indicates that the RNP and RNP' diagnostic plots using material balance time function will shift the plots the right (later) by factor of 2 during linear flow regime.

Rearranging Eq. (b.21), we know that

$$t_{D,p} = \frac{1}{2}t_{eD,p} \quad\text{...(b.22)}$$

Substituting Eq. (b.22) into (b.18) to get

$$t_{D,p} = 2.46\left[\frac{1}{2}t_{eD,p}\right] = 1.23t_{eD,p} \quad\text{......................................(b.23)}$$

Hence, the constant rate time function will be larger than the material balance time function by a factor of 1.23 during linear flow regime.

Comparing Eq. (b.23) with (b.18), it indicates that material balance time function will shift constant pressure response to be closer to constant rate response, but still do not overlay completely. This implies that when plotting RNP and RNP derivative by

using material balance time function, a multiplier correction factor of 1.23 is required to convert completely the constant pressure plots to the constant rate plots.

To summarize, during linear flow period, using material balance time will shift constant pressure time function to the right by a factor of 2. However, it will not convert the constant pressure to constant rate perfectly because the constant rate time function is larger than constant pressure time function by a factor of 2.46. This indicates that the constant rate time function will still larger than the material balance time function by a factor of 2.46 / 2 = 1.23.

B.3 Distance of investigation

Now, let's consider a distance of investigation equation for linear flow in constant pressure condition shown in Eq. (b.24).

$$x = 0.159 \sqrt{\frac{k t_{elf}}{(\phi \mu c_t)_i}} \quad \dots\dots\dots\dots\dots\dots\dots\dots\dots\dots\dots\dots\dots\dots\dots\dots\dots\dots\dots\dots\dots(b.24)$$

Where t_{elf} is the actual time in days at the end of linear flow seen as a deviation from a 1/2 slope trend on log-log plots.

Note that the relations among the dimensionless time functions derived earlier are also applicable with dimensional time function. Eq. (b.25) shows dimensional form of Eq. (b.22).

Linear flow

$$t = \frac{1}{2} t_e \dots \ \dots \ \dots\dots\dots\dots\dots\dots\dots\dots\dots\dots\dots\dots\dots\dots\dots\dots\dots\dots\dots(b.25)$$

Where t is a constant rate time function, and t_e is a material balance time function used to convert constant pressure response to virtual constant rate response.

Substituting t and t_e in Eq. (b.25) with t_{elf} and t_e with $t_{e,elf}$ respectively to have

$$t_{elf} = \frac{1}{2} t_{e,elf} \dots\dots\dots\dots\dots\dots\dots\dots\dots\dots \ \dots\dots\dots\dots\dots\dots\dots \ \dots\dots(b.26)$$

Where $t_{e,elf}$ is material balance time in days at the end of 1/2 slope linear flow as seen on log-log RNP and RNP' versus material balance time plots.

Substituting Eq. (b.26) into Eq. (b.24) we have

$$x = 0.159 \sqrt{\frac{k(t_{e,elf})/2}{(\phi \mu c_t)_i}} \quad \dots\dots\dots\dots\dots\dots\dots\dots\dots\dots\dots\dots\dots\dots\dots\dots\dots\dots\dots\dots\text{(b.27)}$$

Finalize Eq. (b.27) to get

$$x = 0.1125 \sqrt{\frac{k(t_{e,elf})}{(\phi \mu c_t)_i}} \quad \dots\dots\dots\dots\dots\dots\dots\dots \quad \dots\dots\dots\dots\dots\dots\dots \quad \dots\dots\dots\dots\dots\text{(b.28)}$$

Eq. (b.28) must be used to calculate distance of investigation instead of Eq. (b.24) when material balance time directly read from the log-log RNP plots is used instead of the actual time.

B.4 Observations

First, let's recap the dimensionless time function used to derive the distance of investigation equation shown below (Wattenbarger et al., 1998).

$$t_{Dy_e} = \frac{0.00633kt}{(\phi \mu c_t)_i x^2} \quad \dots\dots\dots\dots\dots\dots\dots\dots\dots\dots\dots\dots\dots\dots\dots\dots\dots\dots\dots\dots\dots\text{(b.29)}$$
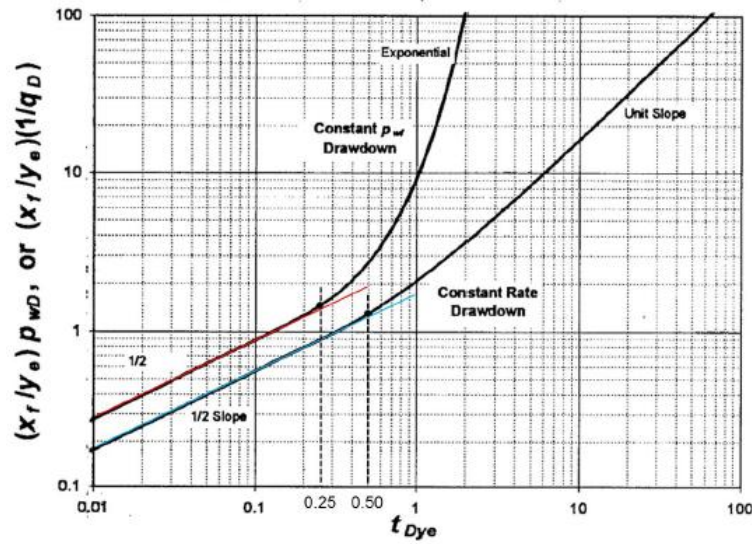
where x is the distance from fracture.

Figure B. 1: tDye assumption for distance to boundary equation

From Figure B.1, the time corresponding to the distance to boundary are assumed at $t_{Dye} = 0.50$ for constant rate, and $t_{Dye} = 0.25$ for constant pressure. Note that these values are defined as the departure time that can visually see on log-log plots, and not the first points that deviated from the 1/2 slope straight line.

The distance to boundary equations are then derived by substituting these values into Eq. (b.29) and solve for y_e. Eq.(b.30) and (b.31) show the equations for constant rate and constant pressure cases, respectively.

$$x = 0.113 \sqrt{\frac{kt_{ehs}}{(\phi \mu c_t)_i}} \quad \dots\dots\dots\dots\dots\dots\dots\dots\dots\dots\dots\dots\dots\dots\dots\dots\dots\dots\dots\dots\dots\dots\dots (b.30)$$

$$x = 0.159 \sqrt{\frac{kt_{ehs}}{(\phi \mu c_t)_i}} \quad \dots\dots\dots\dots\dots\dots\dots\dots\dots\dots\dots\dots\dots\dots\dots\dots\dots\dots\dots\dots\dots\dots\dots (b.31)$$

Here, it should be noted that the assumed t_{Dye} for constant pressure and constant rate cases are separated by a factor of 2. However, we've shown earlier that the constant rate and constant pressure time function are separated by the factor of 2.46, not 2 as assumed.

89